CHALMERS
UNIVERSITY OF TECHNOLOGY

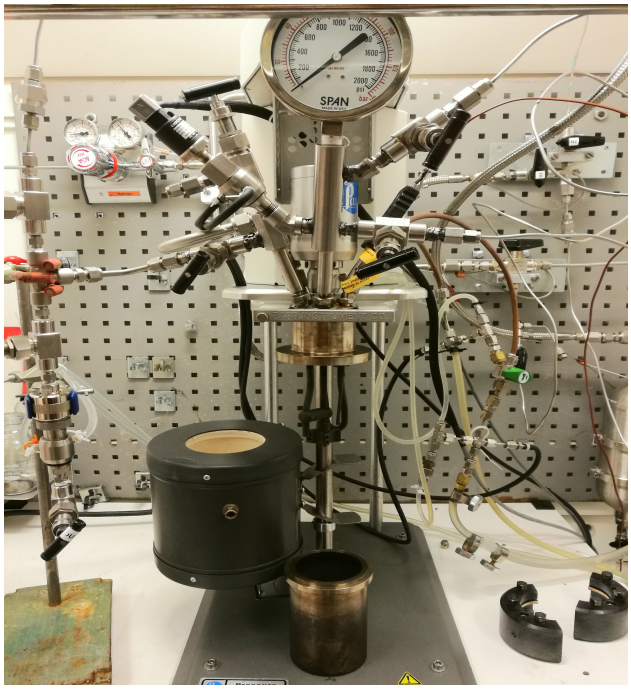

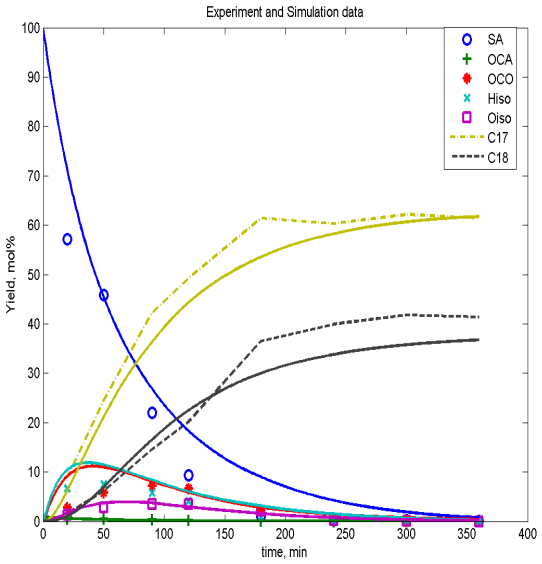

Experimental and kinetic modelling study of hydrodeoxygenation of tall oil to renewable fuel

Master's thesis within the Innovative and Sustainable Engineering program

Katarina Landberg

Department of Chemistry and Chemical engineering
CHALMERS UNIVERSITY OF TECHNOLOGY
Gothenburg, Sweden 2017

Master's thesis 2017

Experimental and kinetic modelling study of hydrodeoxygenation of tall oil to renewable fuel

Master's thesis within the Innovative and Sustainable Engineering program

Katarina Landberg

CHALMERS
UNIVERSITY OF TECHNOLOGY

Department of Chemistry and Chemical engineering
Division of Chemical engineering
Chalmers University of Technology
Göteborg, Sweden 2017

Experimental and kinetic modelling study of hydrodeoxygenation of tall oil to renewable fuel
Master's thesis within the Innovative and Sustainable Engineering program
Katarina Landberg

Supervisor: Derek Creaser and Prakhar Arora, Department of Chemistry and Chemical engineering
Examiner: Louise Olsson, Department of Chemistry and Chemical engineering

Master's Thesis 2017
Department of Chemistry and Chemical engineering
Division of Chemical engineering
Chalmers University of Technology
SE-412 96 Gothenburg
Telephone +46 31 772 1000

Cover: Reactor used in experiments and modelling results constructed in matlab.

Typeset in LaTeX
Gothenburg, Sweden 2017

Abstract

With the increasing greenhouse effect there is a requirement for developing renewable energy and fuels. The petroleum industry is therefore striving to find new ways of creating biomass based fuels to reduce the carbon footprints of their products. One way this is done is to mix in forestry based hydrocarbons into the fossil fuels. A source of these hydrocarbons is tall oil which contains fatty acids. These have high oxygen content which reduces the cold flow properties and chemical stability of the fuel. This oxygen can be removed by a catalytic hydrodeoxygenation (HDO) process. The pure HDO route produces alkanes and water while the parallel routes of decarbonylation or decarboxylation produces alkanes with CO and CO_2 respectively. By modelling the reaction, an improved understanding may be obtained of the relevant reaction routes and how they influence product selectivity depending on the reaction conditions.

A conventional sulphided $NiMo/\gamma - Al_2O_3$ catalyst was prepared and used in HDO reaction experiments with stearic acid, a component in tall oil, as the reactant. Six experiments were conducted at different conditions to obtain a variety of data. One base experiment at a temperature of 300°C, pressure at 50 bar hydrogen and 5 wt.% of feed stearic acid in a dodecane solvent was performed. Two experiments were performed with either higher or lower temperature while two were with either higher or lower pressure and one experiment was performed with a lower amount of stearic acid in the solvent.

The experiments were conducted in a high pressure batch reactor with a stirring rate at 1000 rpm. Internal and external mass transport resistances were negligible and the reactor was considered to operate with ideal mixing. Liquid samples were collected after different reaction times and analyed in a GC-MS. One gas sample was collected at the completion of each experiment and analysed in a GC.

The reactions were assumed first order with respect to the reactants in this initial attempt to model the process. Seven reactions were modelled in Matlab; stearic acid to octadecanal, octadecanal to different intermediates which further reacted to alkenes and finally to either octadecane or heptadecane. Reference reaction rate constants together with activation energies and weighting factors were optimized to fit the model predicted products yields to the experimental results. Despite challenges with experimental precision, the model was able to fit the experiments reasonably well and was able to predict when the selectivity changed to either heptadecane or octadecane depending on the reaction conditions. Experiment liquid sample analyses giving poor material balances tended to cause poorer model predictions of mainly the intermediates octadecanol and heptadecene. The model predictions of gas composition were not strictly validated against experiment measurements, but the gas analysis results were used to consider which reaction routes were dominant in the system.

Sammanfattning

Med en ökande växthuseffekt kommer ett behov att utveckla förnyelsebart bränsle. Oljeraffinaderier strävar därför att hitta nya sätt att skapa biomassa-baserat bränsle för att minska klimatavtrycket från deras produkter. Ett sätt är att blanda in träbaserade kolväten i fossila bränslen. En källa till dessa är tallolja som i sig innehåller fettsyror. Dessa har en hög syrehalt vilket minskar "cold flow"-egenskaper samt bidrar till kemiskt labilt bränsle. Syret kan reduceras med hjälp av katalyserad hydrodeoxygenering (HDO). Den rena HDO-vägen producerar alkaner och vatten som biprodukt medan de parallella reaktionerna; decarboxylering och decarbonylering producerar alkaner med CO_2 respektive CO. Genom att modellera reaktionen kan en ökad förståelse fås för de relevanta reaktionsvägarna samt hur de influerar selektiviteten för produkterna beroende på reaktionstillstånden.
En konventionell sulfiderad $NiMo/\gamma - Al_2O_3$ katalys förbereddes och användes i HDO-experimenten med stearinsyra (en komponent i tallolja) som reaktant. Sex experiment gjordes vid olika tillstånd för att få variationer av data. Ett basexperiment utfördes vid temperaturen 300°C, trycket 50 bar samt 5 wt.% stearinsyra i dodecane. Två experiment med högre respektive lägre temperatur samt två experiment med högra respektive lägre tryck utfördes. Ytterligare ett experiment utfördes med lägre mängd stearinsyra i lösningen.
Experimenten utfördes i en högtrycks-satsreaktor med en mixinghastighet på 1000 rpm. Det interna samt externa masstransportmotståndet försummades och reaktorn antogs ha ideal omblandning. Vätskeprover togs vid olika reaktionstidpunkter och analyserades i en GC-MS. Ett gasprov togs vid slutet av varje experiment och analyserades i en GC.
Reaktionen antogs vara av första ordning med avseende på reaktanterna i ett initialt försök att modellera processen. Sju reaktioner modellerades i MATLAB; Stearinsyra till octadecanal, octadecanal till olika intermediärer som i sin tur reagerade till alkener och slutligen antingen till octadecane eller heptadecane. Reaktionskonstanter tillsammans med aktiveringsenergier samt viktade faktorer optimerades för att anpassa modellens förutsägda produktmängd till de experimentella. Även om utmaningar tillkom med precision av experimenten klarade modellen av att anpassa sig till experimenten ganska bra och kunde förutspå när selektiviteten skiftade mellan produkterna beroende på de experimentella tillstånden. Modellens förutspådda gas-sammansättning kunde inte valideras fullt mot experimentella mätningar, men resultatet från gasanalyseringarna användes för att anse vilken reaktionsväg som dominerar i systemet.

Acknowledgements

I would like to take the opportunity to give special thank to my supervisor Derek Creaser for helping me. I could not have done it even a bit without you. I would also like to specially thank my supervisor Prakhar Arora who helped me with the experimental par. You were always at hand when I needed you and I am glad you were able to put up with me with a smile during the project. I would like to give thank to Olivia Sweeney and Houman Ojagh for all the extra help during the project. Last but not least I would like to thank the other master thesis students and all my friends that I gained during my time at Chalmers for all the joy and encouragement and my family for supporting my decisions in life and helping when I doubt myself. I could not have done it without you.

Katarina Landberg, Gothenburg, 2017

Contents

1
Introduction

1.1 Background

The world is facing several environmental challenges. One of these is the increasing greenhouse effect due to the amount of emissions of greenhouse gases. The increase of greenhouse gas emissions is continuing globally but for some countries, they are beginning to stabilize[1]. To counter the trend of increasing emissions, the EU has established goals for decreasing the emissions and using renewable resources. The 20-20-20 goal, where the amount of renewable energy should increase by 20 percent and the energy consumption should decrease by 20 percent by 2020 is an established vision. Regulations to reduce emissions from fossil fuels have also been introduced to force industries to focus on using renewable energy sources[2][3].

Renewable feedstocks are considered CO_2 neutral because the release of CO_2 into the atmosphere is countered by its uptake by the vegetation during its lifetime. Renewable feedstocks tend also to have low NOx and SOx content which is released into the atmosphere during energy production and causes acid rain[4][5].
Renewable energy sources such as vegetable oil, animal fat or oils from the forest industry can today be used as fuel. However, unless the vegetable oils are recovered from organic waste, their usage competes with the food sector. Industries such as fuel producers are beginning to incorporate renewable feedstocks into their production to reduce the carbon footprint of their products. Such an example is when bio-fuels are mixed with fossil fuels to produce more environmentally friendly types of gasoline and diesel. In Sweden, companies from the forest and petroleum refining industries work together to produce renewable products. The Swedish refinery Preem is producing their Evolution Diesel containing bio-fuels based on tall oil which is recovered from the black liquor in the pulp and paper industry[6][7].

Tall oil contains fatty acids, such as palmitic and oleic acids, resins and sterols, which have high oxygen content. This oxygen needs to be removed in order to improve the cold flow properties, stabilize the fuel and to produce hydrocarbons miscible with the fossil fuels[8][9][10].
Hydrodeoxygenation (HDO) removes the oxygen in the presence of hydrogen gas, where it is released as water. In deoxygenation, the oxygen can also be removed by decarboxylation (HDC) and decarbonylation (DEC) where respectively CO and CO_2 are released as by-products. These processes requires less H_2 for deoxygenation compared to HDO as long as CO or CO_2 does not react further. This can

be beneficial for industries lacking hydrogen, but it comes at the cost of a loss of carbon[9][10][19][11].

The reaction mechanism of HDO is complex and research has been performed to model the reaction and its kinetics[12][13][14]. With a kinetic model, it is possible to gain a deeper understanding of the importance of competing reaction routes and how they vary with the reaction conditions. Furthermore, with a mathematical model predictions can be made of experimental results that provide flexibility to scale up processes where time and money is limited.

1.2 Aim

The aim of this master thesis, which is divided into two parts, is to create a kinetic model of the catalytic HDO process of tall oil in MATLAB, which should explain the kinetic process of HDO based on experimental results.
Some experimental data already existed at the start of the project and this was used to develop an initial basic model. New experiments were carried out with varied parameters such as pressure, temperature and starting concentration in order to obtain more varied data to refine and improve the model.

The starting reactant used in the experiments was stearic acid and no dimethyl disulphide (DMDS) was added to the feed to avoid additional side-reactions, involving its decomposition, from occurring. The reaction was carried out with a sulphided $NiMo/\gamma - Al_2O_3$ catalyst, with a single formulation to further simplify the study. A high pressure PARR batch reactor with a volume of 300 ml was used for the experiments.
The kinetic model should describe the consumption of reactants, production of products as well as the intermediate species in primarily the liquid phase. The gas phase was also analysed to a lesser extent, to gain further insight in the reactions occurring leading to different gas phase products. Some studies on modelling exists but none with the conventional hydrotreating catalyst such as sulphided $NiMo/\gamma - Al_2O_3$.

The most important questions that may be answered from the results of the project include:

- Which reaction routes occur during HDO of Stearic acid?
- What restrictions are valid and could be used for a model of the process?
- Will the analysis of gas phase be helpful for the construction of the model?
- What system of reactions and form of rate expressions are required to fit the model accurately?

1.3 Limitations

The model should be kept simple in the beginning of the project which means adsorption, desorption and surface reaction rates on the catalyst will not be modelled. The model will include only overall reaction rates based on liquid phase conditions. The internal and external transport limitations are assumed negligible as a start.
Because the aim of the experimental part is to obtain basic data for different parameters, sulphiding agents will not be added during the experiment. Experiments will however begin with a pre-sulphided catalyst. The decomposition of sulphiding agents consume hydrogen during the reaction time, and this would be difficult to include in the model at first.
As mentioned in the aim, the majority of the experiments will be carried out with stearic acid to start with cleaner and simpler reaction routes and product compositions.
The solubility of hydrogen in dodecane is modelled with a Henry´s constant estimated from separate phase-equilibrium simulations.
The reaction rate are assumed to be of first order with respect to all reactants in this first attempt at modelling.

2

Theoretical Background

To develop a model of the hydrodeoxygenation process and a kinetic model, knowledge about the process and the reaction mechanism of HDO needs to be obtained. Because a reactor setup and catalyst preparation played an important role in the experimental procedure, knowledge about these areas is also necessary.

2.1 Bio-fuels

Biomass from plants is considered CO_2 neutral due to the CO_2 uptake during their lifetime through the photosynthesis process. They are also in contrast to fossil oil low in sulphur and nitrogen content which leads to lower emissions of NOx and SOx when used as a fuel[4].
Bio-fuels can be divided into 1^{st} generation and 2^{nd} generation fuels. Biofuels today are still dominated by 1^{st} generation bio-oils such as triglycerides extracted from edible biomass and therefore compete with the food sector[10]. Triglycerides can be separated into glycerine and fatty acids methyl esters (FAMEs) through transesterification with an acid or a base catalyst[10]. FAMEs have a high density, boiling point and are unstable. They degrade over time during storage and can damage combustion engines and clog filters due to the high oxygen content. Hence, they are mixed into fossil fuels with limited concentration and thus rarely used in their pure form as fuels[15].

An example of a 2^{nd} generation fuel is forestry-based bio-fuels, which do not compete with the food sector or for land use[10]. All fatty acids, even if it is FAMEs or forestry -based can be hydrotreated to remove oxygen. 2^{nd} generation based oil that is converted into hydrocarbons is often called green or renewable diesel. Green diesel has similar characteristics and chemical composition as a fossil diesel and is compatible with existing engines[15]. The product has a low density and a high cetane index which means that higher amount of green diesel can be mixed in low-value fossil fuels to obtain different fuel products[15].
The green diesel from fatty acids however, has a high cloud point which may block the fuel filter or valves in the engine when operated in cold climates. The hydrocarbons from the fatty acids have a higher melting point compared to fossil hydrocarbons and become a waxy solid at lower temperatures. Even though green diesel can be used as a pure fuel after being treated with isomerization which lowers its cloud point, it is usually mixed with a fossil fuel[15][16].
One specific 2^{nd} generation bio-oil is tall oil. Tall oil is a by-product from Kraft

pulping processes where it is extracted from the black liquor. The black liquor is created in the boiling process of wood chips together with NaOH[17][7]. The crude tall oil (CTO) can be further distilled to tall oil fatty acids (TOFAs) or distilled tall oil (DTO). The fatty acids from tall oil contains chains of between 14 and 24 carbon atoms which is similar to the hydrocarbon length of fossil diesel fuels[15]. In table 2.1 the quantities of different fatty acids in crude tall oil are presented. The composition data is taken from Anthonykutty et al.[8].

Fatty acid	**Percentage in CTO**	
Type	Free	Bonded
Palmitic acid	4.37	0.083
Margaric acid	0.83	0.021
Stearic acid	1.66	0.021
Oleic acid	17.88	0.33
Octadecadienoic acid	11.85	0.79
Linoleic acid	11.43	0.75
Other fatty acids	13.93	2.66

Table 2.1: Percentage of different fatty acids in crude tall oil (CTO)

The hydrocarbon chains are, as stated earlier in this chapter, a product from hydrotreatment of fatty acids where oxygen is reacting with hydrogen[10]. The hydrotreatment process and its reaction routes are further explained in section 2.2.

2.2 Hydrodeoxygenation process

Oxygen removal from fatty acids is performed by hydrodeoxygenation (HDO). Here, oxygen heteroatoms are eliminated in various steps in a hydrogen rich environment to form water. The reaction mechanism of HDO is complex with its various routes and possible product selectivity depends on the type of catalyst and reaction conditions[10][15].

2.2.1 HDO reaction scheme

A requirement for fatty acids to be hydrodeoxygenated is that hydrogen is available to attach to the oxygen and form an aldehyde intermediate. The aldehyde can continue on through the HDO route or further react via decarbonylation (DEC) where the oxygen is removed as carbon monoxide[18][10].
Parallel to the HDO (and DEC) route, the oxygen can be removed by decarboxylation (HDC). Here, the resulting product, like that for DEC, is an alkane with one carbon less than that from the pure HDO route and the by-product is CO_2. Besides these main reaction routes there are two secondary reactions that can occur in the process: water-gas shift and methanation[18][10]. These five main reactions are explained in more detail below.

Hydrodeoxygenation
The conversion of fatty acids to hydrocarbons through the HDO route is shown in eq.2.1.

$$R - COOH + 3H_2 \rightarrow R - CH_3 + 2H_2O(g) \tag{2.1}$$

Although the hydrogen consumption is significant, the only by-product is water which is harmless. This route is most applicable for industrial sites where hydrogen is produced as a side product from other processes or is easy available in larger quantities from other sources [11]. Hydrocarbons produced via the HDO reaction retain the same carbon chain length as the original fatty acid which is desirable as briefly mentioned in chapter 2.1.

Decarboxylation
In decarboxylation (HDC) the carboxylic group is removed from the fatty acids thermodynamically by forming CO_2 and alkanes are produced directly[19]. The reaction is presented in eq.2.2.

$$R - COOH \rightarrow R - H + CO_2(g) \tag{2.2}$$

In contrast to the HDO process, hydrogen is not needed for this reaction to occur making it preferable in processes where there is a shortage of hydrogen. The drawbacks are that CO_2 is produced and, the carbon chain is shortened[15].

Decarbonylation
The decarbonylation (DEC) process proceeds parallel to the HDO route after an intermediate step where aldehyde is formed. Here the oxygen is removed, in the same way as the HDC step, as carbon monoxide, see eq:2.3.

$$R - COOH + H_2 \rightarrow R - H + CO(g) + H_2O(g) \tag{2.3}$$

Less hydrogen is consumed in this reaction compared to HDO but CO is formed.

Methanation
Carbon monoxide and carbon dioxide can further react with hydrogen to form methane and water, see eq.2.4.

$$CO(CO_2) + 3H_2(4H_2) \longleftrightarrow CH_4 + H_2O(2H_2O) \tag{2.4}$$

The compounds inside the parenthesis show the reaction for carbon dioxide[19]. Even though less hydrogen is consumed in the DEC and HDC reaction routes, if a large portion of the resulting carbon oxides react further by methanation, a larger net quantity of hydrogen may be consumed compared to the pure HDO route[15].

Water-gas shift
Finally, the last reaction that can occur is the water-gas shift (WGS) presented in eq.2.5.

$$CO + H_2O \longleftrightarrow H_2 + CO_2 \tag{2.5}$$

In WGS, carbon monoxide reacts with water to form hydrogen and carbon dioxide. This is a reversible reaction which can proceed in either direction, depending on which of DEC or HDC is dominant and the reaction conditions[19].

2.2.2 Reaction routes in detail

For further explanation of the reaction routes mentioned above, a more detailed scheme is presented in fig. 2.1. Stearic acid is used as the reactant fatty acid in this scheme but this reaction route is typical for all similar fatty acids as observed in other studies[18][4][10].

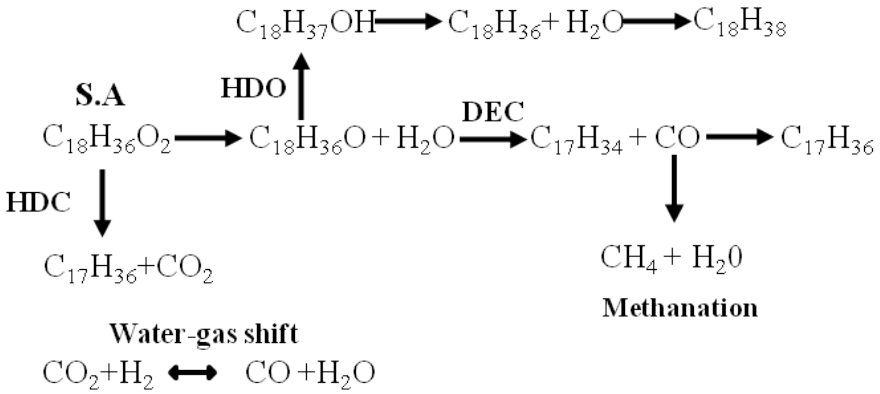

Figure 2.1: Reaction route of HDO of Stearic acid

Stearic acid (S.A) reacts with hydrogen to form the aldehyde 1-octadecanal and water as a by-product[18][10]. When 1-octadecanal further reacts through the DEC route it forms the alkene heptadecene and carbon monoxide which can continue on to form methane by the methanation step. Further hydrogenation gives the alkane heptadecane (C17). If instead the aldehyde reacts through HDO, the alcohol 1-octadecanol is formed[10]. Octadecanol further reacts with hydrogen to form water and the alkene octadecene. Finally the alkane octadecane (C18) is formed from the alkene[18][10].
Due to the different reaction routes and possible further reactions of carbon monoxide and carbon dioxide, the reaction scheme is considered complex. Research involving kinetic modelling of HDO has been attempted to gain more knowledge about the process[9][13][14].

2.2.3 HDO modelling

Kinetic modelling of HDO has been performed by various researchers in order to achieve a deeper understanding of the reaction mechanism. Kumar et al. performed experiments on Stearic acid with a $Ni/\gamma - Al_2O_3$ catalyst at different temperatures, catalyst loading and stearic acid concentrations. Only the liquid phase was modelled and external mass transport resistance was neglected with the knowledge that the conversion of stearic acid did not vary significantly with the speed of agitation at impeller speeds around 1000 rpm[9].
Bie et al. models the surface reaction steps as a part of the reaction rate equation. They performed experiments on methyl palmitate and some of its intermediates over a Rh/ZrO_2 catalyst, with different temperatures at 80 bar and different pressures at 300°C. Here, neither external nor internal mass transport limitations were considered and the hydrogen consumption was taken in consideration for the modelling[13].

In the study Bie et al. the kinetic parameters where optimised by minimizing the sum of square errors between the modelled concentrations and the experimental values to obtain a fitted model. 95 % confidence interval T-test and R-square values were used to evaluate the degree of model fit. Only the major reaction steps were modelled[13].
Kumar et al. also models the major reaction steps and used power law rate expressions. They calculate the activation energy for the different reaction rate constants by plotting the Arrhenius equation and using mean square regression methods. The concentration of stearic acid is calculated with the estimated kinetic parameters and compared to the experimental concentration of stearic acid reaction[9].

2.3 Catalyst

Besides having a complex reaction scheme, the catalyst composition and its properties has an important influence on the HDO process.
A catalyst functions in such a way that it provides an alternative reaction pathway where the activation energy barrier of a reaction is lowered. For a heterogeneous catalyst the reactants adsorb and form products that desorb from the surface. By this alternative pathway, the catalyst may also serve to change the selectivity of a reaction[20].
A proposed simplified catalytic cycle for HDO and DEC reactions of stearic acid over a $NiMo/\gamma - Al_2O_3$ is presented in fig. 2.2. As stearic acid is the reactant used in the project and the reactant used to describe the reaction routes it is used here as well. The catalyst is a sulphided $NiMo/\gamma - Al_2O_3$ as it is also the catalyst used in this project. The cycle shown in fig. 2.2 is based on other cycle presentations with similar fatty acids and catalysts[18].

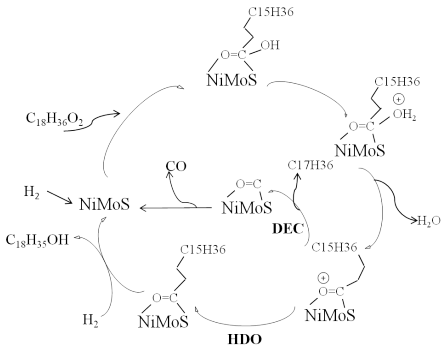

Figure 2.2: shows a simplified catalytic cycle for HDO of stearic acid over $NiMo/\gamma - Al_2O_3$

Hydrogen is added to the sulphided $NiMo/\gamma - Al_2O_3$ catalyst and the reactant is adsorbed on the catalyst surface. Water is desorbed and the two competing DEC and HDO routes can occur. Either heptadecane is desorbed or thereafter CO is desorbed in order to obtain the original catalyst structure. For the pure HDO route hydrogen is adsorbed and octadecane is desorbed.

Catalysts exist in both heterogeneous and homogeneous form which means that the catalyst is either in the same or in a different phase as the reactants and products, respectively[20]. Only heterogeneous catalysts will be described from this point on.

2.3.1 Catalyst structure

There are conventional and non-conventional types of heterogeneous hydrotreating catalysts. Conventional hydrotreating catalysts such as $CoMo/\gamma - Al_2O_3$ and $NiMo/\gamma - Al_2O_3$ need to be presulphided whilst the non-conventional supported noble metal catalysts such as Pt, Pd and Rh do not, although they can be more expensive and suffer from deactivation by poisoning by sulphur compounds[13].
The structure of a catalyst can vary. It may be an unsupported metal catalyst. These often have problems with sintering of the metals which causes the active surface area to collapse. If a stable surface area is needed, then a support can be introduced. Common types of supports are: oxides like $\gamma - Al_2O_3$ which is a transition state of Alumina, Silica and zeolites which is crystalline modification of silica-alumina or carbon[20].
Alumina is an inexpensive support with slight acidity and it can have a relatively high surface area. Higher surface area is preferable due to the possibility of gaining more activity as more active sites can be deposited on the catalyst surface and the active metals are used more effectively. Zeolites can be obtained in different combinations of Si-Al and having different pore sizes and geometry. Carbon is usually used in organic reactions e.g. hydrogenation[20].
In a reaction such as the hydrodeoxygenation where oxygen is released, it can readsorb on an active site and hence cause poisoning of the catalyst. According to literature, the conventional hydrotreating catalysts are most active in their sulphided state, and thus oxygen released during HDO may replace sulphur and cause deactivation[20].
A promoter can be added to the catalyst to e.g. stabilise the surface area even further and to avoid metal migration. The promoter can also weaken the metal-sulphur bond and increase the sulphur vacancies, which are considered to be the active sites on these catalysts for the HDO process[13][9]. For the two conventional catalyst examples mentioned earlier ($NiMo/\gamma - Al_2O_3$, $CoMo/\gamma - Al_2O_3$) Nickel and Cobalt function as promoters[20].

2.3.2 Different catalysts and their effect on the HDO process

The catalyst composition and properties has an important effect on its performance. Although no such investigations have been done in this project, knowledge regarding the effect of the catalyst is important background. Two established HDO catalysts are sulphided $NiMo/\gamma - Al_2O_3$ and $CoMo/\gamma - Al_2O_3$[21]. Their properties and characteristics are well known and they are inexpensive compared to other catalyst systems[20]. Experimental studies have been performed on both the alumina support itself, addition of the active metal molybdenum and further addition of the promoters, Nickel and Cobalt respectively[21][18][12][22].

Comparing the pure support (Alumina) with the sulphided promoted catalyst (from now on named NiMo-Al or CoMo-Al), Laurent et al. saw that the promoted catalyst gave higher conversion of a carboxylic group. NiMo-Al resulted in having higher activity and selectivity towards DEC compared to CoMo-Al[21][4].
When comparing NiMo-Al against Mo-Al, studies have shown that Mo-Al favors the pure HDO route over DEC but the activity is slightly lower than for NiMo-Al[12][18]. Sulphidation, as explained earlier, is carried out to maintain stability and generate active sites. Therefore sulphiding agents (e.g. H_2S and DMDS) are often added during experiments to prevent oxidation of the catalyst[23]. By adding DMDS it can decompose to H_2S by consuming H_2 and thus become a competitive reaction to HDO[10].
When studying the effect of different nickel loadings on alumina without the metal molybdenum, Kumar et al. found that with higher acidity the selectivity towards the HDO path is increased. This can be achieved with increasing nickel to a certain degree[9]. The overall nickel seems still to shift the selectivity towards DEC and increased the reaction rate significantly[9].
When using a zeolite or a noble metal instead like Pd or Rh, the system favored HDO more than DEC. According to Kumar et al. the conversion of stearic acid was large over a zeolite catalyst.
Studies from e.g. Kumar et al. and Brillouet et al., based on experimental analysis of the gas phase with a NiMo-Al catalyst, showed that only CO is detected, except for CH_4, as products. This can be due to that either decarboxylation does not occur at all or the CO_2 is entirely converted to CO through the water-gas shift reaction. However, according to theoretical calculations, the water-gas shift step seems to be thermodynamically disfavoured compared to DEC[9][18]. Although other studies have shown that CO_2 can be observed in the gas phase[12]. Brillouet et al. conducted an experiment with CO_2 in feed to observe if the concentration would increase, but from the product analysis no change was observed which strengthened their belief that only DEC is the alternative route to the pure HDO[18]. This is why only DEC is mentioned as the alternative route to the HDO process in this section and not HDC.

2.4 Analysis methods

GC

Gas chromatography is used for analysing gas samples in order to obtain gas composition. The sample is evaporated in an injector and brought to a column by a carrier gas, which should have a very low oxygen and water content. Different species in the sample gas are separated by their volatility and this results in them having different retention times inside the column. The species are transported, often with a make-up gas, and registered in a detector which can be of different types such as flame ionization (FID) or thermal conductivity (TCD) detectors depending on the type of gas to be analysed[24][25].
Prior to analysing a sample gas, a calibration with a relevant reference gas is fed to the GC apparatus. This is used by the software to compare and register the analysed peaks of gas species [25].

GC-FID
Flame ionization detector (FID) combusts the gas in a hydrogen/air flame which ionizes the gas species. Organic compounds can be analysed with FID due to the ease of ionizing C-H bonds. The ions produce an electrical signal which is measured in the FID apparatus to differentiate the species[26].
GC-TCD
Thermal conductivity detector (TCD) uses two parallel tubes to measure the gas composition. The carrier gas is heated in one tube and the gas to be analysed in the other. The heat loss rate from coils in the tubes, which is a function of the gas thermal conductivity, is compared to analyse the gas composition. The carrier gas is used as a reference, and it is often a gas with high thermal conductivity, such as helium, as these are seldom included in the sample gas.
TCD can detect both organic and inorganic compounds compared to FID lacked the ability to analyse inorganic. Therefor other gases such as nitrogen or hydrogen can be detected[27][28].
GC-MS
Mass spectrometry (MS) can be used to determine a gas composition by separating the gaseous species by their molecular masses. This is done with an ion source where the sample is vaporised and ionized.
The ions go through the mass analyser which uses an electrically induced magnetic field to separate the ions based on their mass-to-charge ratio (m/z) and the resulting signal is registered by a detector. The detector data is analysed in a computer software with a library of compounds to obtain the composition of a sample[29][24].
ICP-SFMS
When promoting or loading catalysts an accurate amount of different metals or elements on the support is important. Small changes can shift the activity of the catalyst and affect the outcome of the reaction[14][9]. With ICP-SFMS (inductively coupled plasma sector field mass spectrometry) elements and their concentration on the catalyst support is measured in their ionized state. The ionizing step is performed with plasma formed by heating gas until electrons move freely away from the atom[30]. A filter uses magnetic and electrostatic differences to separate the elements by their mass-to-charge ratio[24].
Brunauer-Emmet-Teller (BET) theory
With BET theory the surface area of porous materials can be measured. The catalyst is cooled under vacuum conditions with nitrogen which is physisorbed to the porous surface at a temperature of -195°C. As the nitrogen is dosed continuously in small amounts to the porous solid, the saturation pressure is reached in each step and the amount of N_2 adsorbed is monitored. Nitrogen is psysisorbed until a monolayer is formed before multilayers begin to form on the previous monolayer. The volume of adsorbed N_2 (V) is continuously measured throughout the process which gives a volume distribution[31].
The required amount of adsorbate (Vm) to cover one monolayer of the surface is calculated with the experimental values of V and the corresponding P from BET isotherm equation, shown in eq: 2.6.

$$\frac{P}{V(P_0 - P)} = \frac{1}{V_m} + \frac{(c-1)}{V_m c}(\frac{P}{P_0}) \tag{2.6}$$

Where P is the total pressure, P_0 is the vapor pressure of nitrogen and c is a constant. With V_m and the area of the adsorbate molecule (A), eq: 2.7 below is used to calculate the surface area (SA)[20].

$$Sg = \frac{A * V_m * N_A}{V_A} \tag{2.7}$$

The BET surface area is achieved by dividing SA with the sample mass. By decreasing the pressure, nitrogen is desorbed inside the pores

3
Modelling Methods

This chapter will be about construction of the model in Matlab. Its parts and the assumptions, decisions and restrictions will be presented and discussed.

3.1 Creating the model

For the modelling, the desired outcome is a prediction of the concentration profile of the consumption of the starting reactant, which here is stearic acid, and the production of intermediates and final products over time. This is then compared to the experimentally observed concentrations.
The main equation that is solved to obtain the concentrations of the different compounds over time is the mole balance. The reactor used for the experiments is assumed to behave as an ideal batch reactor and the mole balance equation for such is presented in eq: 3.1 below.

$$\frac{dN_j}{dt} = \sum (\nu_{ij} * r_i) * W \tag{3.1}$$

Here, ν is the stoichiometric coefficients for component j in reaction i and r is the reaction rate for the corresponding compound´s consumption or production. W represents the catalyst loading in the reactor. N_j is the number of moles of component j in the reactor. This differential equation is solved using the ODE15s function in Matlab together with the initial moles of the reactant and hydrogen. The starting concentration of stearic acid in the solvent n-dodecane was calculated to obtain the number of moles. The starting moles of hydrogen in the reactor was calculated using the ideal gas law with the set total pressure in the reactor during the experiments. The next step for the differential equation to be solved was to model the reaction rate. First order reactions with respect to the liquid phase reactant concentrations were assumed to apply. Such rate equations may not be appropriate in all cases, but the objective of this work was to examine how well or poorly they may perform. The reactions takes place on the surface of the catalyst and the solid catalyst is assumed to be completely wetted so the reactions are occurring in liquid phase conditions.

The general reaction rate equation is presented in eq: 3.2

$$r_i = k_i * \Pi(C^{\mu}) \tag{3.2}$$

Here k_i is the reaction rate constant which is obtained from Arrhenius equation (see

eq: 3.3).

$$k = k_{ref} * e^{\frac{Ea}{R}*(\frac{1}{T_{ref}}-\frac{1}{T})} \tag{3.3}$$

The reference temperature (T_{ref}) was chosen as 300°C and T is the operating temperature for the reactor. This form of the Arrhenius equation (eq: 3.3) was used to prevent correlation between the pre-exponential factor and activation energy. The unknown parameters in this equation are k_{ref} (rate constant at reference temperature) and Ea (activation energy). Values of these were tested until the modelled concentration profiles fitted the experimental ones closely. Further explanation is presented below in section 3.2.

The second term in eq: 3.2 is the mathematical product of the reactant concentrations for the specific reaction raised to the order of the reaction (µ). The concentrations are obtained from eq. 3.1 as the simulation is running based on the initial given moles of stearic acid and hydrogen. Because assumptions were made about the liquid phase conditions, the concentrations of the gas components were obtained in liquid phase. The equation used for this calculation is shown in eq: 3.4 below.

$$C_g = \frac{N_g}{\Sigma(N_g)} * \frac{P_{tot}}{he} \tag{3.4}$$

Ng is the moles of the gas components in the reactor and he is the Henry's constant. For hydrogen which is a very volatile molecule, the concentration in the liquid phase is obtained from knowing the solubility at the reaction conditions i.e. obtaining Henry's constant.

3.1.1 Solubility calculations for obtaining Henry´s law constant

Henry´s constant is expressed in eq: 3.5 where P_{H2} is the partial pressure of hydrogen and C_{H2} is the concentration of the gas component in liquid phase.

$$P_{H2} = he * C_{H2} \tag{3.5}$$

The solubility of hydrogen in n-dodecane which was the solvent used in the experiments with a concentration above 95 mol% were calculated in HYSYS. A simple flash system in Aspen HYSYS (see fig A.1 in Appendix) was designed. Three fluid packages (Peng-Robinson (P-R), TST and SRK) were tested due to suggestions from internet sites comparing similar systems. As fig. A.1 in appendix shows, one gas stream with pure hydrogen and one liquid stream with pure n-dodecane is mixed and transported with the help of a pump to keep the desired pressure in a flash tank which separates the streams into a gas phase and a liquid phase.
This was done for the three pressures of 40, 50 and 60 bar and temperatures of 280, 300 and 320°C. The mole fraction of hydrogen in liquid phase and gas phase was recorded. Results from HYSYS of predicted molar fractions in liquid and gas phase showed that the values from the P-R package were in between those of the other

two packages as presented in table 3.1 below.

P(bar)/T($°C$)	40	50	60
280	0.082	0.102	0.121
300	0.089	0.112	0.134
320	0.098	0.125	0.142

P(bar)/T($°C$)	40	50	60
280	0.915	0.900	0.878
300	0.820	0.852	0.874
320	0.741	0.786	0.817

Table 3.1: P-R prediction of mole fraction of H2 in liquid phase (left) and molar fraction of H2 in gas phase (right)

The liquid molar density of the n-dodecane solution was also obtained from HYSYS and with the liquid molar fractions of hydrogen, the concentrations of hydrogen in n-dodecane were calculated and are presented in table 3.2. The predicted liquid molar density was 3.195 $kmol/m^3$.

P(bar)/T($°C$)	40	50	60
280	260.4	325.3	387.6
300	285.0	358.5	428.4
320	313.1	398.1	452.1

Table 3.2: Concentration $[mol/m^3]$ of H_2 in liquid phase

In order to obtain Henry's constant for one combination of pressure and temperature a function file was created with the concentrations above in it. The calculated concentration was obtained by eq.3.6

$$C_{calc} = P_{H2}/he_{ref} * e^{\frac{\Delta H}{R}*(\frac{1}{T}-\frac{1}{T_{ref}})} \tag{3.6}$$

Where he_{ref} was calculated from the eq. 3.5 with the concentration at 50 bar and 300°C in table 3.2 and the partial pressure for hydrogen at 50 bar. T_{ref} is the reference temperature of 300°C and ΔH is the solvation enthalpy of hydrogen which was set as an initial guess. Matrices of T and P were given in the function file for to finally get a calculated concentration. To obtain Henry's constant from eq: 3.7 residual and least square calculations was done with the optimisation function lsqnonlin in matlab.

$$he = he_{ref} * e^{\frac{\Delta H}{R}*(\frac{1}{T}-\frac{1}{T_{ref}})} \tag{3.7}$$

This function calculates concentrations and the ones in table 3.2 to obtain a value of he_{ref} and ΔH that gives the smallest differences in concentration.

3.2 Kinetic modelling

Returning to modelling the reaction rates, the reactions needed to be chosen. From the theory section 2.2 the possible reactions in the hydrodeoxygenation process were

presented. Because model development began before any experiments had been done on stearic acid, which was used as the feed compound, an experiment with oleic acid was used.
Also, in the beginning, no gas analysis results were available as well so the gas phase was not taken into consideration in the same way yet and assumptions had to be made on which reactions that occurred. Five reactions were considered for oleic acid in order to create the model. They are presented in eq: 3.8-3.12.

$$C_{18}H_{34}O_2 + H_2 \rightarrow C_{18}H_{36}O2 \tag{3.8}$$

$$C_{18}H_{36}O2 + 2H_2 \rightarrow C_{18}H_{37}OH + H_2O \tag{3.9}$$

$$C_{18}H_{37}OH + H2 \rightarrow C_{18}H_{38} + H_2O \tag{3.10}$$

$$C_{18}H_{36}O2 \rightarrow C_{17}H_{36} + CO_2 \tag{3.11}$$

$$CO_2 + 4H_2 \rightarrow CH_4 + 2H_2O \tag{3.12}$$

Eq: 3.8-3.10 is through HDO with stearic acid and 1-octacedanol as intermediates and octadecane as the final product together with water. Eq: 3.11 is the HDC route of stearic acid and eq: 3.12 is methanation of CO_2. These were chosen as starting reactions but all were however not used in the final model. As experiments was conducted with stearic acid the DEC route was chosen instead of HDC based on claims in the literature that DEC was more thermodynamically favored[18] The intermediate steps of production and conversion of 1-octadecanal was also added since its formation was observed in the later experiments and its inclusion would allow a more complete model of the HDO process to be obtained. Other intermediate species such as heptadecene and octadecene were also added later on as well. The final complete set of reactions will be presented in the result and discussion part of this report. The stoichiometric variables were added as a matrix together with the order of reaction matrix for each species in the Matlab program.
The values of the kinetic parameters (k_{ref} and Ea) for each reaction were set as initial estimates as the result was compared to the experimental concentration profiles which were also incorporated into Matlab as well.

3.2.1 Parameter fitting

Optimisation of the kinetic parameters was performed with the objective to minimize the residuals between calculated and experimental concentrations. This was done with two optimisation functions in Matlab; namely lsqnonlin, a gradient search method and simulannealbnd, a global search method using a simulated annealing algorithm. The optimisation was carried out for all experiments which results in kinetic parameters designed to fit all experiments as closely as possible. Hence all the experiments were checked with the guessed values of K_{ref} and Ea before parameter fitting was introduced.
In order to evaluate the fit of the kinetic model, other than from inspection of the figures, an R -square value was calculated in the program.

3.3 Experimental incorporation

The measured experimental concentrations against time were added in an excel file for each species. The pressure drop and the top-up of hydrogen were also added in two columns. weighing factors are also added to each species.
The experimental files were loaded in Matlab where time, concentration, pressure drop and top-up pressure were called. Weighting factors that could be set for the components were also loaded into the program. These factors can be changed to give different sample points more or less importance which will force the model to fit them better i.e the weighing of residuals of component with low concentrations are increased in order to obtain a good fit compared to components with higher concentrations.
The moles of hydrogen were calculated with the ideal gas law depending on the operating pressure for each experiment and the initial moles of stearic acid n-dodecane were given.
These values are called upon in another function file that plots the results of the concentration profiles, the gas compositions, the comparison of the experimental concentration profiles and the calculated and finally the total pressure in the reactor over time. This pressure is obtained based on calculations from sample withdrawal in the model.

3.3.1 Modelling sample withdrawal

Every time a sample was withdrawn from the batch reactor the pressure dropped since some gas and liquid was drained. This pressure drop needed to be included in the model to obtain an accurate result. The pressure was recorded before a flush sample was taken and again after the real sample was taken, to calculate the pressure drop. The hydrogen top-up was calculated based on the difference in pressure after sample withdrawal and the pressure needed to reach the operating conditions.
There was hence two parts in the code. The first part was for the pressure drop and the second part for the hydrogen top-up. With the pressure differences the difference in volume of gas and liquid was obtained and was used to calculate the new catalyst loading, due to some loss of catalyst in the withdrawal process, volume of gas and volume of liquid that remained in the system. With the volume difference the moles of gas components and moles of liquid components after sample withdrawal was calculated. The change in gas was also calculated depending on the top-up of hydrogen after sample withdrawal.

4

Experimental method

4.1 Catalyst preparation and characterisation

A batch of bimetallic catalyst with nominal loadings of 5% Ni and 15% Mo on γ-alumina as support was synthesized by the method described below.
First, calibration of a pH meter was performed using standard buffer solutions of pH 4 and 7. By wet impregnation, 12.83 g of alumina was added to 200 ml of distilled water with a constant stirring of 500 rpm. The pH of the solution was around 7. The solution needed to be acidic, with a pH of around 4, which was achieved by adding 10 wt.% of HNO_3. The required amount of molybdenum precursor ($(NH_4)_6Mo_7O_{24} \cdot 4H_2O$) was dissolved in the distilled water. Then it was added to the alumina solution simultaneously as the acid to maintain a constant pH of 4.
The solution was added to two round bottom glass bottles which was cooled by liquid nitrogen and attached to a freeze-dryer (scanvac cool safe) for 24 h to remove the excess water (for visual understanding, see fig. appendix A). After drying the catalyst powder, it was put in an oven for calcination. The catalyst powder was calcined at 450°C for 2 h with a heating ramp of 5°C/min to remove volatile components.
The next step was to load nickel onto the catalyst. The $Mo/\gamma - Al_2O_3$ powder was mixed in 150 ml of distilled water and the measured pH was 4. In order to achieve a satisfactory loading of Ni, the pH needed to be increased to 9. This was done by adding NaOH continuously until the solution was stabilized at pH9.
The desired amount of Ni loading was 5% so the required amount of the precursor used ($Ni(NO_3)_2 \cdot 6H_2O$) was added to 20 ml of distilled water. This was then added simultaneously with an appropriate amount of NaOH to the catalyst solution, because the Ni solution lowered the pH. During this procedure, lumps appeared but with an increase in the stirring rate, the majority of the lumps disappeared. The solution was again poured into two bottom glass bottles and was freeze-dryed in liquid nitrogen for 24 h.
The last step was to calcine the catalyst powder again at 450°C for 2 h with a heating ramp of 5°C/min.

ICP

A freshly prepared sample of the catalyst was sent to the company ALS for ICP analysis. This was done to determine the actual obtained loadings of molybdenum and nickel. The target contents were 5% Ni and 15% Mo, but the actual loadings were 14.2% Mo and 4.39% Ni.

BET
The surface area of the catalyst was obtained by BET analysis with a Micromeritics Tristar 3000 instrument. 0.3g of fresh catalyst was heated up in a vacuum oven to remove all moisture prior to the analysis. This was done to be able to compare the catalyst activity to some degree by comparing the BET result with other studies with the same type of catalyst. The surface area of the catalyst was found to be 145.4 m^2/g. Comparing this surface area with Snare et al. and Brillouet et al. it is smaller. The area is not far from Snare et al. (195 m^2/g) and one explanation could be that their catalyst had a lower loading of nickel on it. Loading a metal will reduce the surface area[19]. For brillouet et al. the surface area was 257 which is much higher, but the amount of Ni and Mo on their support was not mentioned[18].

4.2 Experimental procedure

The experimental procedure is separated into three parts which starts off with a description of the reactor used in the project followed by the procedure to pre-sulphide the catalyst in the reactor. This is done to convert Mo on the catalyst, from its oxide to active suphide form. The last part is the experimental procedure to carry out the actual reactions where six experiments were conducted.

4.2.1 Reactor system

The reactor used in the experimental part of this project is a high pressure reactor from PARR instrument company. It is assumed to be an ideal batch reactor with complete mixing which means the reactions are taking place throughout the reactor volume, under the same conditions and at the same rate. The reactor vessel, with a volume of 300 ml, is sealed with a gasket made of Teflon and split-ring cover clamps tightened by cap screws.
The gasket has a working temperature of up to 350°C before it starts to leak due to the pressure build up. Other materials of the gasket such as graphite can be used when the temperature of the experiment exceeds 350°C[32].

A schematic view of the reactor and its different parts are shown in figure 4.1. A photo of the reactor is shown on the title page.
Hydrogen is added through the gas inlet (1) and when an inert atmosphere is desired nitrogen is added instead. To analyse a gas sample, a sample container is connected to the outlet (2). The pressure relief line (3) is connected to the ventilation system and has a rupture disc attached to prevent the pressure from exceeding the safe operating pressure for the reactor[33].
The sample outtake is connected at (4) and goes through (6) where the samples are taken out during experiments. Nitrogen is injected through (5) to clean and flush out sample leftovers.
The reactor volume is mixed by an impeller. The impeller shaft is hollow with holes at the top of the shaft and at the impeller blades. During mixing, suction builds-up to force gas through the impeller shaft and sparged into the liquid. This enhances the turbulent mixing. A temperature, pressure and stirring rate detector

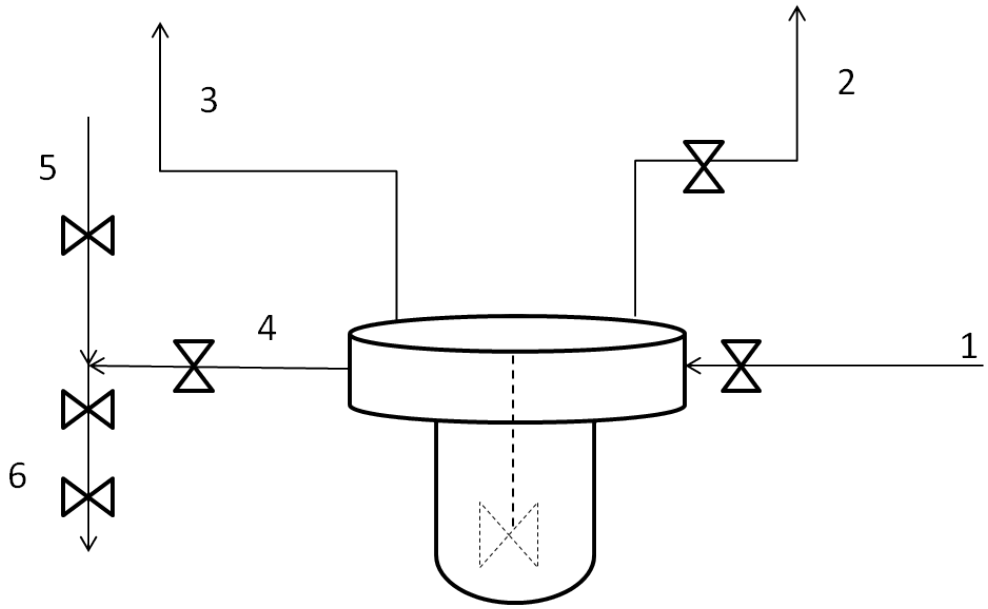

Figure 4.1: Schematic view of reactor system

is attached at the top of the reactor equipment where cooling water is added to prevent over-heating of the impeller motor.

4.2.2 Sulphidation process

Before every experiments, the catalyst needs to be sulphided. This was done in the high pressure PARR batch reactor.
0.5 g of fresh catalyst is added to the reactor vessel together with 0.5 ml of DMDS (dimethyl disulphide). The reactor was closed and tightened and flushed two times with nitrogen to remove oxygen from the system. Then, the system is flushed with hydrogen one time. A pressure test with hydrogen of 10 bar was performed during ten minutes to check if there existed any leakages. The pressure was maintained at 10 bar of hydrogen and the reactor temperature was increased to 300°C. Once the temperature was reached it was increased to 335°C and the reactor was left for 4 h to obtain sulphidation before it was cooled down.
After the sulphidation, the reactor and its contents were left under a low nitrogen pressure until the experiment was conducted. This is to keep the catalyst in an inert atmosphere to prevent its oxidation.

4.2.3 Experimental process

A total of six different experiments were conducted in the batch reactor. The six experimental operating conditions are presented in table 4.1 below where the first row represents the base case.

# of experiment	Temperature (°C)	Pressure (bar)	Stearic acid (wt.%)
Exp 1	300	50	5
Exp 2	320	50	5
Exp 3	300	40	5
Exp 4	300	50	2
Exp 5	300	60	5
Exp 6	280	50	5

Table 4.1: shows the different running conditions of the experiments

For the first experiment 5.68 g (5 wt.%) of stearic acid was measured and added to the catalyst in the reactor. 143.96 ml of n-dodecane and 0.1 ml of DMDS was added to the reactor as well. The reactor was then closed and tightened again and flushed two times with nitrogen and one time with hydrogen. A pressure test was performed here as well with hydrogen at 10 bar for about 15 min to check if any leakage existed.
The reactor was emptied of hydrogen until atmospheric pressure was reached and then the temperature was increased to 300°C. When the final temperature was reached, the stirring was turned on and increased to 1000 rpm. Hydrogen was then added until the pressure reached 50 bar and that was when time zero for the experiment started.

A sample of approximately 2 ml of liquid was taken at that time, which resulted in a 1.5-2 bar pressure drop. The pressures before and after extractions of liquid samples were always recorded. A total of eight samples were extracted during the reaction time and in addition a flush sample, causing a maximum of 1 bar pressure drop was extracted before every sample. After each sample withdrawal, the reactor was re-pressurized to the operating pressure with hydrogen. The last sample was taken after cool down and shut down of the reactor which was done one hour after the seventh sample. The consistency of the number of samples withdrawn and when they occurred differed from experiment to experiment depending on the reaction conditions e.g. for experiments with higher temperature, the conversion of reactants expects to occur quicker hence more samples were taken earlier.

For all experiments except the first, DMDS was not added. Otherwise, the experiments were performed in the same procedure with exception of the temperature and pressure targets and the quantity of stearic acid added as table 4.1 shows. It was planned for one more experiment with a higher wt.% of added stearic acid (8 wt.%) but time for this was not available. Also, the normal procedure for previous experiment was to add DMDS to the reactor to make sure the catalyst stay sulphided during the experiment which was the reason for the addition of DMDS in experiment one.
DMDS was not added to the rest of the experiments because it contributes to more reactions and hydrogen consumption which would have complicated the model. Again due to a lack of time the first experiment could not be repeated without DMDS for better comparison with the other experiments.
When an experiment was finished the stirring was slowed down and a gas sample of

about 10 bar was taken from the reactor and into a stainless steel cylinder of 100 ml. Next, the reactor was cooled down to room temperature while the gas was diluted with hydrogen and nitrogen. At room temperature the reactor was flushed a couple of times with nitrogen before opening. 2 ml of the remaining liquid was taken as the last sample and the cleaning of the reactor was the last step. No spent catalyst was saved for further analysis.

4.3 Sample analysis

After the experiment was performed, the samples, both liquid and gas, were analysed in order to determine the composition of each sample taken at varying times during the experiment.

4.3.1 Liquid sample analysis

The liquid samples were heated up in a water bath to liquefy stearic acid. 1 ml of each sample was put in another sample tube and 200 μl pyridine was added in order to keep the samples in liquid form. The samples were then centrifuged. 200 μl of each sample was added to vials together with 30 μl of Bis(trimethylsilyl)trifluoroacetamide (BSTFA). BSTFA is added to the samples in order to shield the carboxylic and hydroxylic groups and improve their separation in the GC. The samples were left standing for 24 h before analysis to allow BSTFA to fully react. If the samples had been left much longer, the compounds could be decomposed by the BSTFA. The liquid samples were analysed in an Agilent 5777A MSD 5890B GC GC-MS.
The sample compounds were quantified with a flame ionization detector (FID), which has been calibrated with pure compounds and identified with the MS.
Peaks from the MS detector were compared in the software to a library (NIST MS) to identify the compounds. The area of these peaks from FID were transferred to an excel file and with the help of calibration data and the initial molar percent of stearic acid the molar percent of each compound was calculated. These molar percentages were then plotted in excel but also added to an excel file used to contain experimental data for the modelling.

4.3.2 Gas sample analysis

The goal was to analyse the gas in the GC (SCION 456-GC) but when the experiments begun the GC was neither equipped with the appropriate columns nor properly configured to achieve separation of the gas phase components. Professional help was obtained to properly configure the GC and a general method was developed to achieve the desired separation.
In the developed method the temperature in the GC is increased to 40°C and held there during 3 minutes. Then the temperature ramping was set to 10°C/min until it reached 120°C which was the operating temperature for 15 minutes. The carrier and make-up gas for the TCD was Argon while the make-up gas for FID was Helium. Hydrogen and air are supplied to the FID for burning to be able to operate.

A calibration gas that was at hand was run in the GC by first flushing the GC with it for 30 seconds to clean the system. The gas composition is presented in table 4.2 below.

Gas species	Concentration %
CO	0.508
Co_2	0.505
CH_4	0.532
Propane	0.520
H_2	1.019
N_2	97

Table 4.2: Calibration gas composition. Calibration gas handed by air liquid

The calibration gas analysis result was saved in the GC software to be able to quantify compounds in the gas samples collected from the reactor.
The sample was run the same way as the calibration gas with a 30 second flush before the injector opened. The peaks were compared in the software with the calibration gas and identified. The FID detected the organic compounds such as methane, propane and ethane while the TCD detected e.g. nitrogen, hydrogen, CO and CO_2.
The calibration gas used was not optimal for the current gas composition in the gas sample because it contained both CH4 and CO which could not be separated in the TCD and hence not accurately calibrated. Another problem was that the concentration of hydrogen in the gas sample was much higher than in the calibration gas.

5
Results and Discussion

Results for the final modelled reactions, their parameter values and the six experiments that were conducted are presented below. The discussion of the experiments and modelling results are divided into sections according to the reaction conditions varied. First the results from the base case will be discussed followed by sections dealing with variation of temperature, hydrogen pressure and finally the concentration of stearic acid. After these sections, an overall discussion and summary is presented. One thing that needs to be noticed is that for the GC results, the results of one additional experiment will be shown. Table 5.1 shows the abbreviations that will be used in this chapter for each of the detected compounds.

Abbreviations	Compound
SA	Stearic acid
OCA	Octadecanal
OCO	Octadecanol
Hiso	Heptadecene
Oiso	Octadecene
C17	Heptadecane
C18	Octadecane

Table 5.1: Compound abbreviations

5.1 Final Model

The reactions used to develop the final model together with the estimated activation energies and reaction rate constants are presented in table 5.2 below.
The reaction scheme used is based on theory in literature that decarboxylation would be disfavored compared to decarbonylation (DEC), water-gas shift towards CO_2 is thermodynamically disfavored and the fact that studies showed that methanation occurs[18]. The intermediate reactions are also included.
Once these reactions were decided, the reference reaction rate constants (k_{ref}) were adjusted manually until the model predictions fitted the experimental results somewhat well and thereafter the values were optimised in matlab. Then the activation energies were optimized to further decrease the error. Finally, different weighting factors, explained in section 3.3, in the excel files were set to see if even a better fit could be achieved. The methanation reaction was estimated to have a high k_{ref} after

Type of reaction	Reaction	Ea [kJ/mol]	$k_{ref}[s^{-1}]$
SA to OCA	$C_{18}H_{36}O_2 \rightarrow C_{18}H_{36}O + H_2O$	137	$1.8*10^{-5}$
OCA to OCO	$C_{18}H_{36}O + H_2 \rightarrow C_{18}H_{37}OH$	87	$8.8*10^{-4}$
OCA to Hiso	$C_{18}H_{36}O \rightarrow C_{17}H_{34} + CO + H_2$	88	0.34
OCO to Oiso	$C_{18}H_{37}OH \rightarrow C_{18}H_{36} + H_2O$	0.03	$7.5*10^{-3}$
Oiso to C18	$C_{18}H_{36} + H_2 \rightarrow C_{18}H_{38}$	26	$8.7*10^{-5}$
Hiso to C17	$C_{17}H_{34} + H_2 \rightarrow C_{17}H_{36}$	15	$5.3*10^{-5}$
Methanation	$CO + 3h_2 \rightarrow CH_4 + H_2O$	15	$3.64*10^{-4}$

Table 5.2: Final values of Ea and k_{ref}

the first gas samples had been analysed where only small amounts or no CO/CO_2 were detected while methane were. So assumptions was made that all gas phase carbons was converted by methanation to CH_4. These results are presented and discussed further below.
Because the model tries to obtain a single set of parameter values that fit best for all experiments, it will often not be able to fit perfectly to a certain experiment. By putting more weight on different experiment's concentrations at a certain point, the parameter optimization can be forced to fit that point better. The drawback is that the ability to fit other measured points can be decreased

5.2 Base case

In figure 5.1 the base case experiment is plotted together with the simulated data. The experiment symbols and lines for each component are shown in the legend and the simulated data is represented by the solid lines in the corresponding colours.

The selectivity towards heptadecane is high compared to octadecane for this experiment as can be observed in fig.5.1. This would be because DMDS was added to the reactor, and its decomposition competed with the HDO route for hydrogen. The consumption of H_2 by DMDS is not explained by the model. For the remaining experiments, it was decided to not add DMDS.
The intermediate octadecanal is barely visible in the figure but was detected in the sample analysis as an increase in the beginning of the experiment. The amount of octadecanal was quite constant during the rest of the experiment until the last sample where it was not detected anymore. This indicates that the further conversion into octadecanol or heptadecene occurs directly as octadecanal starts to form. Octadecanol and octadecene have similar concentration profiles through the experiment while heptadecene is produced faster in the beginning. This is due to the selectivity towards heptadecene. The yield of intermediates increases at the beginning of the experiment and thereafter starts to decrease. The reaction from octadecanal to octadecanol and heptadecene respectively occurs quickly and the amount of heptadecene in the first sample is already higher than octadecanal. The reaction from octadecanol to octadecene also occurs quickly.

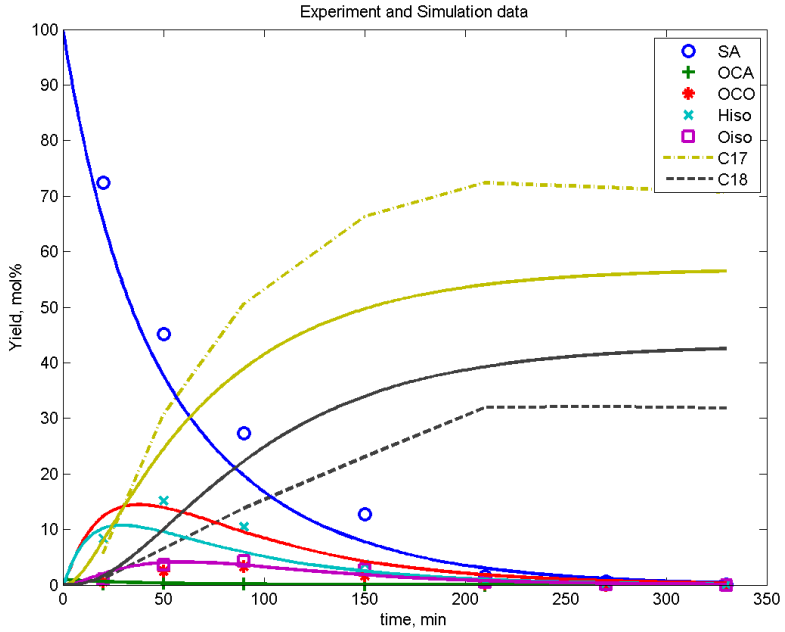

Figure 5.1: Base case experiment with T:300°C, P:50 bar, C: 5 wt.%.

5.2.1 Modelling results of base case

The model predicts 100% conversion of stearic acid which the experiment reached as well. The model seems to fit octadecene and octadecanal well but has difficulties with the final products and the intermediates octadecanol and heptadecene. These are over predicted early in the experiment which could be because the experimental material balance is off. The material balance, which is calculated as the difference between the carbon in the products and the carbon in the reactant, is shown in table 5.3.

Time/Exp condition	20 min (mol%)	120 min (mol%)	330 min (mol%)
T:300, P:50, C:5	92.89	117.70 (150 min)	108.30
T:320, P:50, C:5	73.68	108.0	113.50 (240 min)
T:300, P:40, C:5	81.49	98.98	108.51
T:300, P:50, C:2	99.85	95.33	113.89
T:300, P:60, C:5	65.86	103.40	105.90 (270 min)
T:280, P:50, C:5	86.89	116.41	126.38

Table 5.3: shows the material balance for different experiment at three different reaction times

Because samples were taken at different time intervals for some experiments and due to problems with leakage in reactor which interrupted experiment 2 (higher T), values are taken around the given times shown in table 5.3. As observed, the material balance is rather consistently low at the beginning of the experiments and high in the end. The model is therefore expected to over-predict yields of product in the

beginning and under-predict at the end particularly for the intermediate compounds that were present in low concentrations.
The weighing factors for the base case experiment were increased for octadecanal and octadecene. This was applied for all experiments. Because this experiment had the addition of DMDS which could have changed the selectivity significantly, no other weighting factor was changed in order not to over-emphasize a good fit to this experiment.
Visually the model fits the reactant, stearic acid, and the octadecene intermediate quite well but it cannot handle octadecanol and heptadecene intermediates and the final products. Because of the figure scale it can appear as though the error for the intermediates is small and larger for the products.

5.2.2 Gas analysis of base case

The chromatograms from the gas analysis of the base experiment are presented in figure 5.2 and 5.3 below where the y-axis shows the intensity and the x-axis shows the retention time.

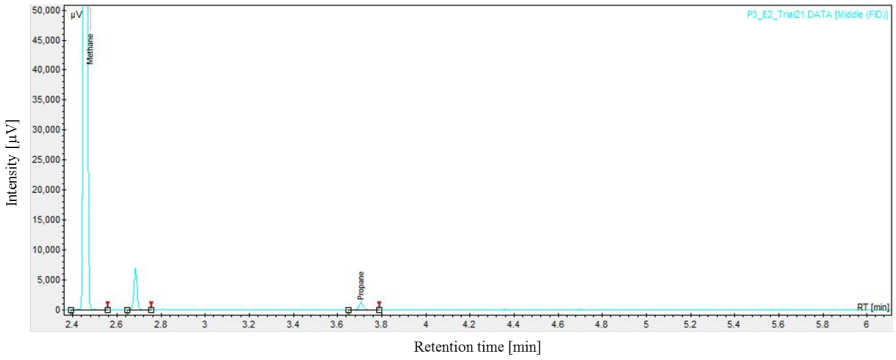

Figure 5.2: FID analysis of final gas from base experiment

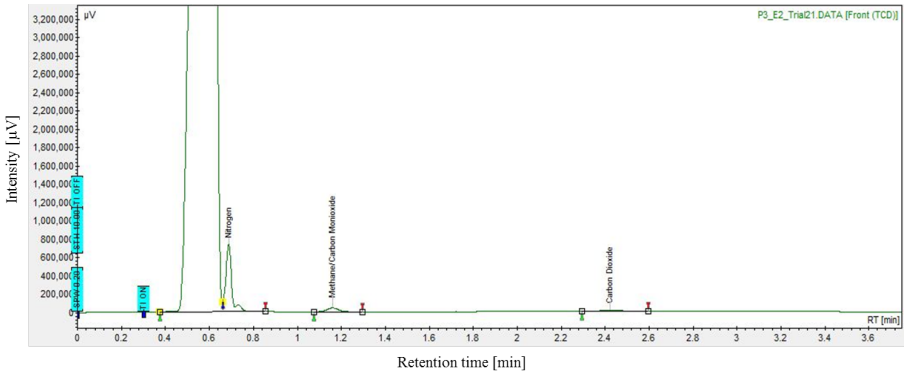

Figure 5.3: TCD analysis of final gas from base experiment

The first peak in fig. 5.2 shows methane, the second is probably ethane and the third is propane. This shows that methane is produced in the system but because DMDS was added for this experiment, methane would have been formed from DMDS decomposition and possibly also the methanation reaction. Ethane and propane are

likely to have been formed by cracking reactions in the system. That is, when carbon chains are split into shorter chains. Even if it is not shown in the results here, both hexadecane and pentadecane were observed in the sample product analysis which then would have been produced by cracking together with ethane and propane. Hexadecane and pentadecane were observed from the liquid analysis but their yields were low at less than 1 mol% which is why their results are not presented.
In fig. 5.3 the TCD results are presented. Here the first peak is with certainty hydrogen. The software was unable to identify the hydrogen because the amount of hydrogen in the gas sample was much higher than the amount in the calibration gas. This caused the retention time for the hydrogen peak to be shifted. The second peak is nitrogen which comes from the fact that the sample cylinder contained N_2 at atmospheric pressure, due to flushing, before filling it with the sample gas.
Here, both carbon monoxide and methane is identified as one peak. This is because the column on the TCD side of the GC was unable to separate them. Also, carbon dioxide is detected. This contradicts the theory about HDC not occurring in the reactor [18]. Then again, HDC could occur due to the lack of hydrogen in this experiment which is used by the DMDS making the decarboxylation route favourable.
The GC chromatograms for the remaining experiments will be in appendix. Table 5.4 below shows the mole % of species in the gas samples for each experiment. N.D stands for not detected and in the TCD, the percentages have been adjusted to give their amounts in the gas without N_2. For FID there were only given the quantity for methane. This is because too small amount of propane was detected and ethane was not identified.

	TCD analysis		FID analysis	
Experimental condition	CO/CH_4(%)	CO_2(%)	CH_4(%)	C_3H_8(%)
T:300, P:50, C:5	1.18	1.98	0.5	0
T:320, P:50, C:5	0.16	N.D	0.07	0
T:300, P:40, C:5	N.D	1.39	0.05	0
T:300, P:50, C:2	N.D	N.D	0.05	0
T:300, P:60, C:5	0.13	1.24	0.06	0
T:280, P:50, C:5	N.D	N.D	0.02	0

Table 5.4: shows the mol% of CO/CH_4 and CO in the gas sample

Due to the uncertainty that arised due to inadequate calibration and not knowing if it is carbon monoxide that was observed or methane, the gas results are not calculated with or used in the model to further develop the reaction routes. Even though this applies, the modelled gas concentration profile is presented in figure 5.4.

As said above, this is just the result that is observed from the predicted liquid concentration profiles. The steps that appear in the profiles result from sample withdrawals and hydrogen top-up. The gas concentration profile will not be shown in the result for the remaining experiments but will be found in appendix A for the readers own interest.

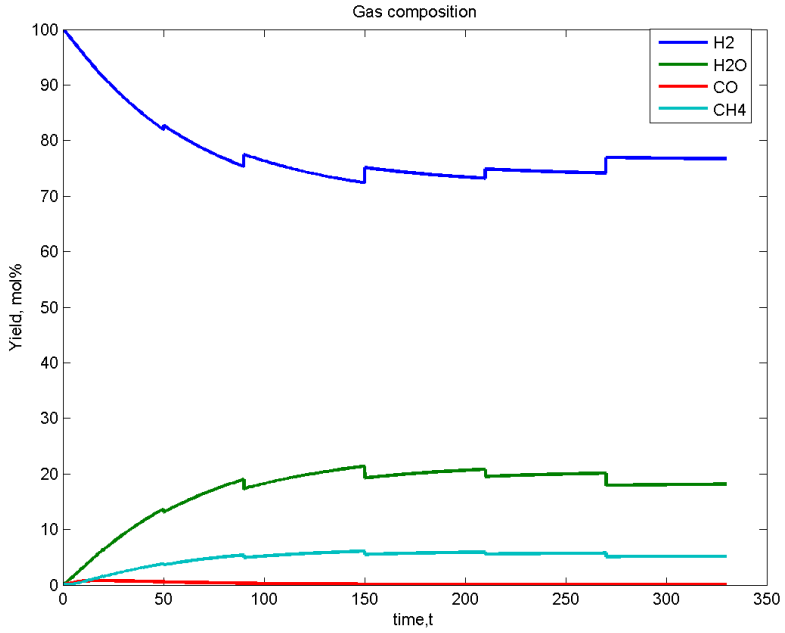

Figure 5.4: Model predicted gas composition over time for the base case

5.3 Temperature dependence

The experiments examining temperature dependence were conducted with an upper temperature of 320°C and a lower temperature of 280°C. The other conditions were set to the base experiment levels with the exception that DMDS was not added.

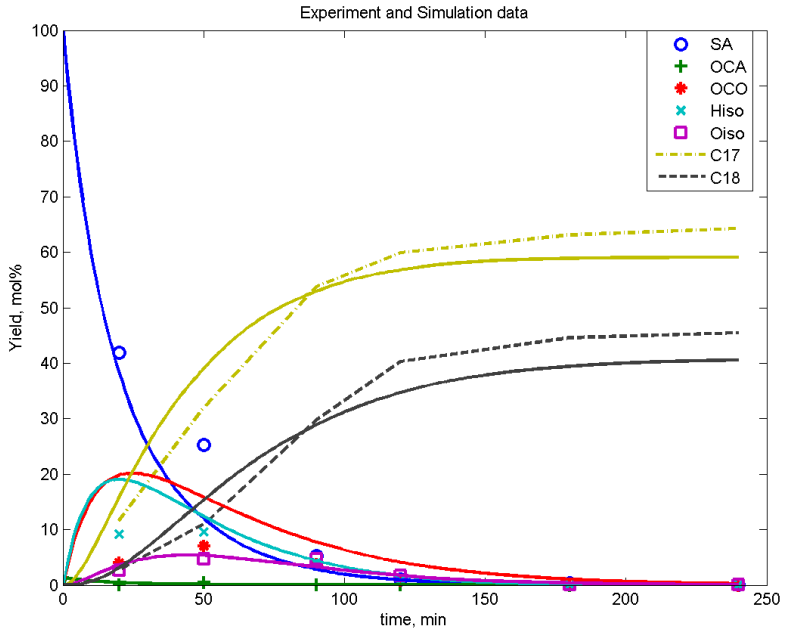

Figure 5.5: High temperature experiment with T:320°C, P:50 bar, C: 5 wt.%.

Figure 5.5 shows the concentration profiles of the higher temperature experiment. Comparing the experimental part of this experiment with the base experiment, a clear observation is that the selectivity towards octadecane is increased. What also can be noticed is that the selectivity towards octadecanol compared to heptadecene has increased which is reasonable.
By having higher temperature, the reaction rate increases which affect the speed of the reactions, as can be observed by the fact that the curves begin to flatten already at approximately 150 minutes compared to the base experiment in which full conversion was not reached until around 220 minutes. This does not necessary mean that the selectivity between the reactions will be affected. As stated previously it is therefore difficult to say if the temperature increase has affected the reaction outcome significantly due to the uncertainty in the base case experiment. What can be observed is the trend that heptadecane is the favoured final hydrocarbon product which probably is due to the nickel content of the catalyst as explained in the theory section.

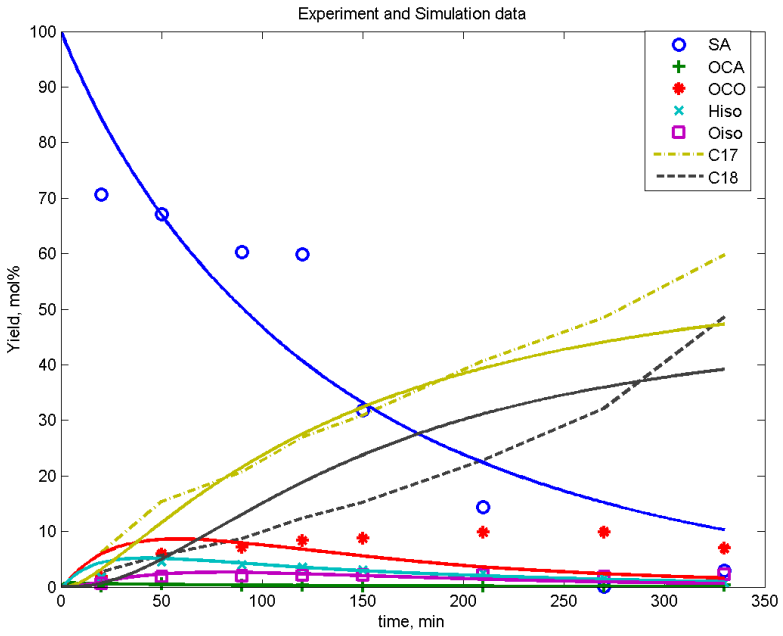

Figure 5.6: Low temperature experiment with T:280°C, P:50 bar, C: 5 wt.%.

Figure 5.6 shows the result of the experiment at the lower temperature. The experiment did not reach full conversion before cool down of the reactor, but trends can still be observed. For instance, the reaction rates were much slower for every compound. What is strange in this experiment is that the speed of reaction suddenly increases after 250 minutes, however this is likely due to experiment error.
Because the selectivity towards octadecane is increased in both experiments with temperature change compared to the base case, and with regards that every other condition is the same in the experiments, conclusions can be made that DMDS actually disturbs the reactions significantly. This means that the base experiment cannot

be fully compared to the other experiments. What also can be observed is that the octadecanol does not reach 100 % conversion at lower temperature which would mean that if the experiment would been run longer, the yield of octadecane would have been increased significantly. This suggests that lower temperature favours the HDO route.

5.3.1 Modelling results

Comparing the simulated concentration profiles with the experimental observations obtained in fig. 5.5, once again it appears as if the model cannot fit the two intermediates octadecanol and heptadecene at the beginning of the experiment. It compensates for the low material balance as can be seen in table 5.3 at 20 minutes, by over-predicting the concentration of intermediates. Contrary to the base experiment, the model seems to be able to handle the final product concentration profiles better and follow the experimental profile trends quite well. This comes to show that the model handles the given reaction routes without disturbance from other side reactions well. The weighting factors in experiment with higher T for octadecanol and heptadecene were increased to see if the model would fit better, which it did. Sadly, by doing this the overall fit for all experiment was worse so the weight factors were set to one again.

For the experiment with lower temperature, the model seems to follow octadecanol and heptadecene quite well in the beginning but not at the end of the reaction time which is opposite of what it did with the two first experiments. This instead results in an under- prediction as can be expected from the too high material balance in table 5.3 at the end of the experiment at low temperature. This would mean that, with a poor material balance octadecanol and heptadecene are the compounds for which the model fits poorly and when the material balance is good, the model fit is better. For these two experiments, the optimization of the activation energy values has high importance. This is due to the fact that the activation energies regulate the variation of the reaction rates with temperature.

5.3.2 Gas analysis

Looking at the results from the gas analysis starting with the 320°C case, the FID (see appendix, fig.A.3) detects methane, propane and again ethane as the second peak. The methane peak for the base case is higher than for the two experiments examining temperature dependence as shown in table 5.4. The methane peak for the lower temperature (see table 4) is much lower than in the two previous experiments. One explanation for the base case would be that DMDS would form methane and hence contribute to the production of methane making it incomparable to the other cases. As can be observed, the base line in fig. A.7 is going up which means that the analysis results cannot be fully evaluated. Why that is will be explained in the overall discussion. However, for lower temperature, the reactions went slower and full conversion was not reached as observed in fig.5.6 which would mean that not as

much methane was produced as for the higher temperature experiment. The trends in the FID results for temperature therefore seem reasonable.
The results for the TCD detector are presented in table 5.4 for both experiments. For experiment with higher temperature, CO/CH_4 was again detected. Either this means that carbon monoxide is formed or it means that the peak is only methane. What is more plausible is that carbon monoxide is formed otherwise methane would not be observed. Here no carbon dioxide is observed which is consistent with the observed results from the liquid analysis which showed higher selectivity towards the HDO route than in the base case.
Comparing row three and row seven in table 5.4 which is the experiment with lower temperature, neither carbon monoxide nor carbon dioxide is detected.
At low temperature, stearic acid did not reach full conversion and the selectivity towards HDO is rather high which mean that there is less carbon products in the gas phase compared to other experiments. No CO or CO_2 was detected in the TCD because FID is more sensitive and can detect lower concentration.

5.4 Pressure dependence

Moving on to the pressure dependence experiments where except for the base case with pressure of 50 bar, two experiments were performed with operating pressures of 40 bar and 60 bar of hydrogen respectively. Figure 5.7 shows the results of the experiment with lower operating pressure.

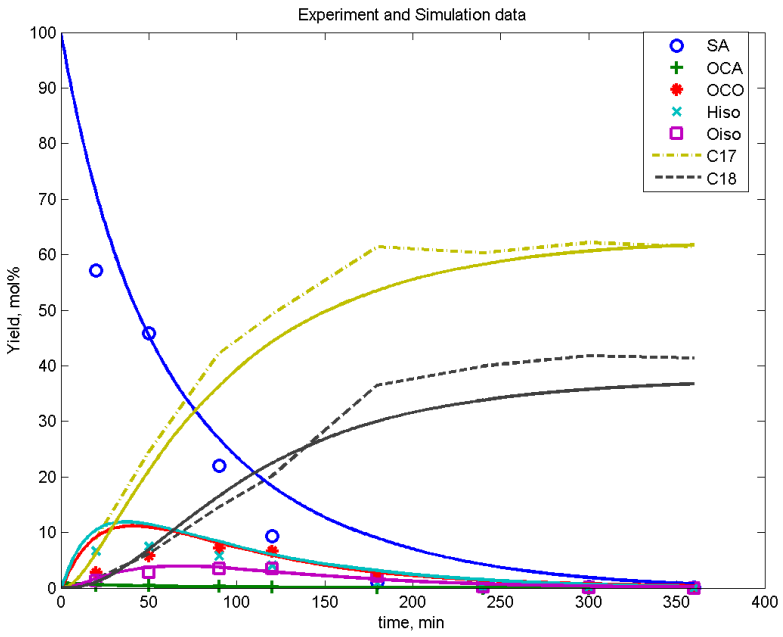

Figure 5.7: Experiment with low hydrogen pressure T:300°C, P:40 bar, C: 5 wt.%.

Comparing this experiment to the base case, the selectivity has changed towards octadecane more. The intermediate reactants for octadecene and octadecanal still seems to have the same profile while for octadecanol and heptadecene the profiles

reach higher and lower concentration peaks respectively. At lower pressure, less hydrogen is present in the reactor which would favour the DEC route. Comparing the experiment with higher pressure (figure 5.8) the hypothesis is shown to be correct. For high pressure experiment the selectivity towards octadecane and hence

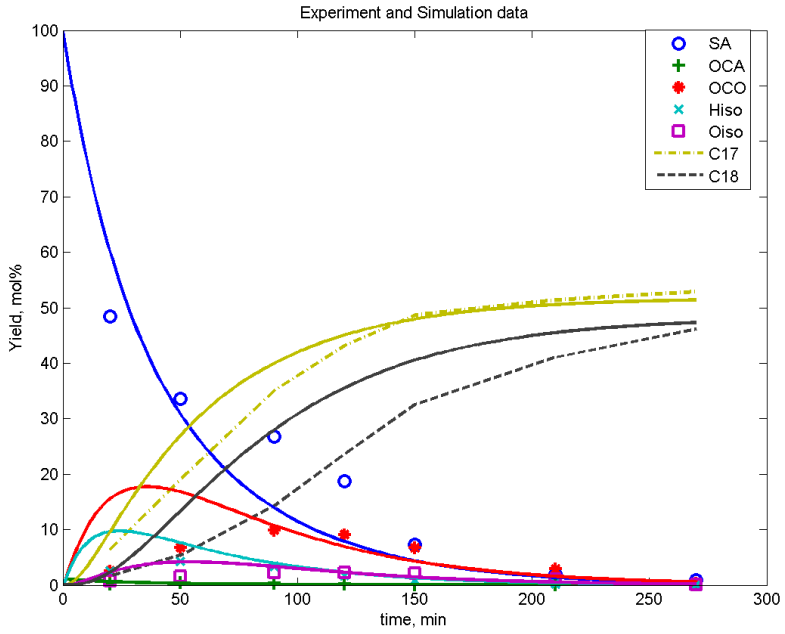

Figure 5.8: Experiment with high hydrogen pressure T:300°C, P:60 bar, C: 5 wt.%.

the HDO route has increased significantly. The octadecanol peak is higher as well. Hence, adding more hydrogen enhances the HDO route but as soon as hydrogen is lacking the DEC route is favoured. If another catalyst, say only $Mo/\gamma - Al_2O_3$ could be used lacking the metal promoter blocking the active sites, maybe the final concentration of octadecane in this case would be much higher than heptadecane as other studies have shown [12][18]. This would be preferable for industries with an abundance of hydrogen due to the desire to retain carbon in the product and the fact that less CO and/or CO_2 by-product is produced.

5.4.1 Modelling results

The model seems to handle the case for lower pressure well with respect to the intermediates. This could be due to the decent material balance presented in table 5.3. The fact that the reaction step from octadecanal to heptadecene is independent of hydrogen (see table 2) whereas the step from octadecanal to octadecanol depends on hydrogen allows the model to correctly predict higher octadecane selectivity at higher pressure. For higher pressure the material balance is off (see table 3) for the intermediates at the start of the experiment, making the model fit poorly. The model seems to add the extra quantity of material lacking in the experiment to octadecanol. Regarding the overall product profiles the model seems to follow the trends in fig.5.7 well. In fig.5.8 the model had trouble to accurate predict the middle

part of octadecane and stearic acid yields but it is capable to pick up their trends in the end.
This is because more weight factors in experiments with higher and lower pressure have been changed. In the lower pressure case, stearic acid and Hiso residuals were given more weight which lead to a better overall model fit which is reflected in the simulated results in fig.5.7. For the higher pressure experiment, more weight was placed on the final products which explains why the model is coping with the trends so well. This did not affect the overall fit of the model negatively either.

5.4.2 Gas analysis

Figure A.4 and A.6 in appendix shows both the FID and TCD chromatograms of experiment with lower pressure and higher pressure respectively.
Methane is detected for both experiments again in the FID together with propane and ethane. Table 5.4 shows no propane but it is due to the small amount detected. More methane seems to have been formed in the experiment with higher pressure which even though it contradicts the liquid analysis where the pure HDO route was clearly favoured the DEC route is also favoured because it goes through the first HDO step. Methane could come from cracking as well which would increase the production. When comparing the TCD results in table 5.4, they differ in gas products as well. For the lower pressure case, carbon dioxide is observed but no other products. This is reasonable due to the lack of hydrogen increasing the chances of decarboxylation to occur. In the case with higher amount of hydrogen in the system, CO/CH_4 is detected together with CO_2. This would mean that even though the HDO route is favoured the parallel HDC or water-gas shift routes still occur. This also explains the higher peak of methane in the FID results which then comes from CO or CO_2. As before this leads to uncertainties in which route that is occurring.

5.5 Stearic acid feed concentration dependence

Only one experiment was done with a different stearic acid feed concentration due to the lack of time in the project. The experiment was performed with a lower amount of stearic acid in the system, at 2 wt.% instead of 5 wt.%. It can still be compared to a certain degree with the base case though. In fig.5.9 a strange behaviour can clearly be observed in the experiment. The oscillating pattern that the two alkane products are making indicates possible errors in the sample analysis or withdrawal. Lower analysis precision, due to the lower concentrations of compounds may have contributed to this variation. Despite this the intermediates and the reactants seem to have the same profiles as could be observed in the previous experiments so it would be most likely the analysis that was at fault. Looking at the experimental profile for heptadecene it is much lower than in the base case while the profile for octadecanol is a bit higher. This is also reflected by the profiles for heptadecane and octadecane having the same yields.
With lower amount of stearic acid one could compare this to the higher amount of hydrogen in the system. The selectivity would as it is does here favour octadecane.

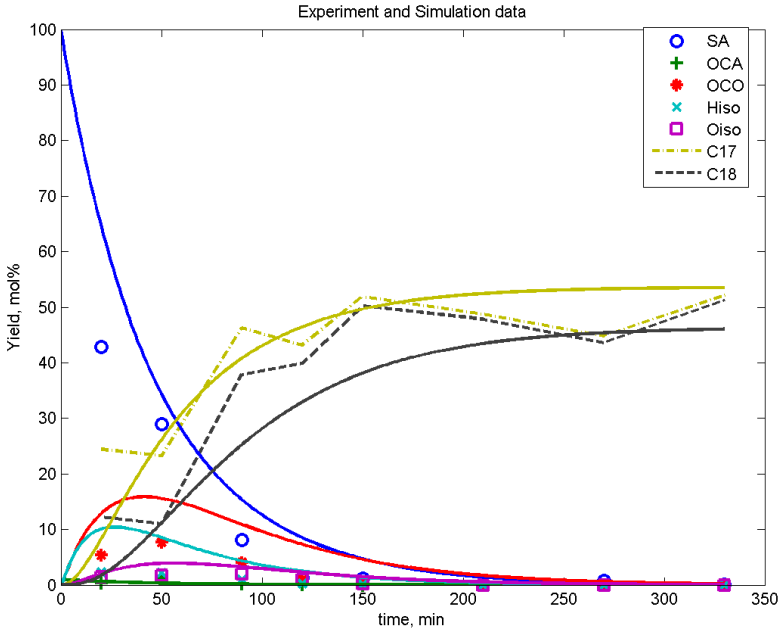

Figure 5.9: Experiment with low stearic acid T:300°C, P:50 bar, C: 2 wt.%.

Comparing the base experiment to this experiment the selectivity towards octadecane has increased significantly and this may be partly due the greater availability of hydrogen due to the lower stearic acid concentration. Studies show that larger fatty acid molecules like stearic acid can strongly adsorb onto the surface of the catalyst and hence inhibit the HDO route because hydrogen adsorption is hindered. With less stearic acid in the system and the same amount of catalyst, the surface would not be covered fully and hence the selectivity towards the HDO route could be therefore increased [14][10].

5.5.1 Modelling results

The modelled concentration profiles in fig.5.9 again have problems with heptadecene and octadecanol but manage to fit the product quite well. It was able to fit octadecane rather well but admittedly not as high as observed for the experiment. If the higher selectivity towards octadecane comes from the reduced inhibition of HDO with lower amount of stearic acid as stated above, the modell does not account for that.
The weighing factors for this experiment were not changed much. It was only octadecane that was weighted more to give emphasis for fitting the high experimental yield that was observed in this experiment.

5.5.2 Gas analysis

The FID gas analysis from experiment with lower amount of stearic acid showed yet again methane. Here the base line deviated as it did in a previous experiment which gives some uncertainty in the analysis results. Methane was observed with

similar peak intensity as previously but in the TCD chromatogram no products were detected as shown in table 5.4. This would mean that carbon monoxide and/or carbon dioxide is fully converted to methane in the methanation step. Both the FID and TCD chromatograms can be found in appendix fig.A.5.

5.6 Overall discussion

When discussing the model fit and the effect the weighting factors have on the model in the previous sections, it is based on the calculated residuals. The residuals are converted to an R square value which tells what fraction of the total variation of the experimental data is explained by the model. This was the value that was checked when the weighting factors were changed. The R square value for the final model is 0.83 which is on the lower side of a good fit. But one must have in mind that it may not entirely be the model per se that is inadequate; it can be also due to inconsistencies of the experiments. Almost all experiments had some uncontrolled deviations resulting from either human error, the DMDS addition or experimental condition errors including reactor or valve leakage. The model fit cannot be fully evaluated due to lack of replicate experiments. If these had been done evaluations if the lack of fit of the model equals the expected variations from experimental errors could be made. There was no time left to redo the first experiment with no addition of DMDS as well as another experiment with higher feed concentration of stearic acid. This could have increased the model fit.

Another Matlab optimization function other than lsqnonlin, namely simulannealbnd, was added to the model. This function starts with the given parameters but unlike the lsqnonlin which uses a gradient search method starting from the starting parameter values, simulannealbnd looks more random and globally over the parameter values searching for values that can lower the residuals. A drawback with the optimization function is that it requires considerably longer simulation times. It gave more random results which could be better but because lack of time this function was not used.

The material balances for the experiments were off in such a way that they were either below 100 % or above as shown in table 5.3. It is reflected in the modelled yields where the model tries to, where the experiment is lacking material, to add it on to the predicted octadecanol and where the model has an excess of material, to decrease on the predicted octadecanol. This can be seen by the fact that the simulated octadecanol is typically higher than the experimental values in the beginning of the experiment and higher at the end, for example in fig.5.8.
The reason why the material balance is off can be because there are other peaks detected in the GC-MS coming from impurities in dodecane or stearic acid that are not quantified. This was confirmed by doing a sample analysis with only stearic acid in dodecane where the same peaks were observed.

Comparing all the experiments to one another, one can see that higher pressure and lower stearic acid favours the HDO route. The higher temperature and the case

with lower pressure have similar concentration profiles where the selectivity clearly favours heptadecane.
In the gas analysis the uncertainty arises with the calibration gas. This makes it difficult to do anything more with the results other than general discussion. The base line is also off at some of the analysis in the TCD which comes from contaminations in the column or leakages. Compounds that have higher boiling points take longer to leave the column and can be left there if the analysis is not run long enough and therefore come out slowly in the next sample run.

As for now the assumptions of first order reactions and the neglected transport limitations still exists. It could be that some reactions have another order dependence which contributes to the lack of fit. The confidence that external mass transfer is negligible is still believed to be valid based on the earlier studies made. The internal mass transfer could play a part in the model fit as well if it cannot be negligible. This theory could be tested by calculations or specialised experiments.
The reaction rates, because no adsorption or desorption was investigated, are normal power expressions without these terms and could also affect the model outcome. The vapour-liquid equilibrium is now calculated with Henry's constant but it seems that this is not a rigorous treatment. This is because dodecane exists in the gas phase as well in the operating temperatures used and the fact that hydrogen is less than sparingly soluble in the liquid at the elevated pressures of the experiments used. Water has also been assumed to be fully vaporised although it is not highly volatile in the experimental conditions used.

6
Conclusion

The final reaction routes used in the Matlab model are presented in table 5.2 in the result part. This reaction scheme was used based on previous reported in literature but as discussed regarding the gas analysis it appears incorrect to neglect both the decarboxylation and water-gas shift routes. This is due to the detection of carbon dioxide in the gas analysis results for some of the experiments. From the gas analysis by FID, methane was always present in the product gas. This means that the methanation route occurs in the system as believed. The TCD detector could not separate CO and CH_4 so the peak detected could be only methane but because methane always was detected in the FID, CO must have been produced. The gas phase was modelled but due to poor calibration of the gas analysis, the predictions were not validated against the experimental measurements.

The model was able to fit the experiment quite well with regards to the general trend of the experimental concentration profiles. It could also follow the variations in the selectivity for the final products (octadecane and heptadecane) with the experimental conditions. However, the model seemed to over or under-predict mainly the intermediate compound octadecanol depending on the bias of the material balance of the experiments. Weighting factors were added in Matlab to force the model to improve the fit of certain compounds at different reaction times. The weighting factors, reaction rate constants and activation energies were optimized to reach a high R-square value.

The sulphiding agent DMDS was added in the first experiment to maintain the catalyst in its sulphided state. This was not added to the remaining experiments with a risk of having complicated reaction schemes. The results showed that the model indeed had complications with the addition of DMDS due to its influence on the experimental results and because it was not accounted for in the model.

A similar research study of stearic acid over $\mathrm{Ni}/\gamma - Al_2O_3$ has been done showing that the external mass transfer resistance could be negligible with a stirring speed around 1000 rpm. This speed is used in this study hence; the external mass transfer resistance has been neglected here as well.

6.1 Future work

For future work, better experiments with more precision should be conducted. Repetitive experiments can increase the model fit validation and better quantify pure experimental errors.

The internal mass transfer resistance should be investigated to further examine if it can be neglected which could be done with calculation. External mass transfer resistance could be validated by experiments with varying speed to ensure it can be negligible at 1000 rpm.

More experiments should be done with octadecanal to validate and get an understanding if DEC occurs only or if the parallel HDC reaction occurs as well. In this way it could be possible to validate whether the water-gas shift reaction also occurs. Model could be expanded to also account for Oleic acid.

The model predictions of gas composition should be validated against experimental measurements. For his, better calibration gases are needed which can calibrate all compounds at their appropriate concentration levels.

Lastly an incorporation of a thermodynamic model to account 'on-line' for the vapour-liquid equilibrium in the Matlab code can be made.

Bibliography

[1] Olivier et al. (2016). Trends in global CO_2 emissions, 2016. *netherlands environmental assessment agency* publ. nr. 2315.

[2] Eu-upplysningen.se, 2016. *Klimatmål för att stoppa global uppvärmning.* [online] Available at: `http://www.eu-upplysningen.se/Om-EU/Vad-EU-gor/Miljopolitik-i-EU/Klimatmal-for-att-stoppa-global-uppvarmning/` [Accessed January-17].

[3] naturvardsverket.se, 2015. *miljoskatter och miljoavgifter.* [online] Available at: `http://www.naturvardsverket.se/Miljoarbete-i-samhallet/Miljoarbete-i-Sverige/Uppdelat-efter-omrade/Styrmedel/Ekonomiska-styrmedel/Miljoskatter-och-miljoavgifter/` [Accessed January-17]

[4] Senol et al. (2006). Reactions of methyl heptanoate hydrodeoxygenation on sulphided catalysts. *Journal of Molecular Catalysis A: Chemical* 268: 1-8

[5] forestry.gov.uk, 2015. *use of wood energy.* [online] Available at: `http://www.forestry.gov.uk/forestry/infd-7m8g28` [Accessed January-17]

[6] Preem.se, 2017.*Preem Evolution Diesel+.* [online] Available at: `http://preem.se/privat/drivmedel/produktkatalog-privat/produkter/diesel/preem-evolution-diesel/` [Accessed January-17]

[7] Sunpine.se, 2016. *From forest to green diesel.* [online] Available at: `http://www.sunpine.se/en/tecknology/` [Accessed January-17]

[8] Anthonykutty et al. (2015). Hydrotreating reactions of tall oils over commercial NiMo catalyst. *Energy Science and Engineering* 3 (4): 286-299.

[9] Kumar et al. (2013). Kinetics of hydrodeoxygenation of stearic acid using supported nickel catalysts: Effects of supports. *Applied catalysis A: General* 471: 28-38.

[10] Coumans et al. (2016). A model compound (methyl oleate, oleic acid, triolein) study of triglycerides hydrodeoxygenation over alumina-supported NiMo sulfide. *Applied catalysis B: Environmental* 201: 290-301.

[11] Santillan-Jimenez et al. (2012). Catalytic deoxygenation of fatty acids and their derivatives to hydrocarbon fuels via decarboxylation/decarbonylation. *Journal of Chemical Technology and Biotechnology* 87 (8): 1041-1050.

[12] Kubicka et al. (2009). Deoxygenation of vegetable oils over sulfided Ni, Mo and NiMo catalysts. *Applied Catalysis A: General* 372: 199-208.

[13] Bie et al. (2016). Hydrodeoxygenation (HDO) of methyl over bifunctional Rh/ZrO_2 catalyst: Insights into reaction mechanism via kinetic modeling. *applied catalysis A: General* 526: 183-190.

[14] Boda et al. (2009). Catalytic hydroconversion of tricaprylin and caprylic acid as model reaction for biofuel production from triglycerides. *Applied catalysis A: General* 374: 158-169.

[15] Donnis et al. (2009). hydroprocessing of bio-oils and oxygenates to hydrocarbons. Understanding the reaction routes. *Topics in catalysis* 52 (3): 229-240.

[16] Li et al. (2014). Preparation of mesoporous activated carbon supported Ni catalyst for deoxygenation of stearic acid into hydrocarbons. *environmental Progress and Sustainable energy* 34 (2): 607-612

[17] Demirbas, A. (2008). Production of Biodiesel from Tall Oil. *Energy sources, part A: Recovery, Utilization, and Environmental Effects* 30 (20): 1896-1902.

[18] Brillouet et al. (2013). Deoxygenation of decanoic acid and its main intermediates over unpromoted and promoted sulfided catalysts. *Applied Catalysis B: Environmental* 148-149: 201-211.

[19] Snare et al. (2006). Heterogeneous Catalytic Deoxygenation of Stearic Acid for Production of Biodiesel. *Ind. Eng. Chem. Res* 45 (16): 5708-5715.

[20] Ross. J. (2011). *Heterogeneous Catalysis: Fundamentals and Applications*. Elsevier.

[21] Laurent et al. (1993). Study of the hydrodeoxygenation of carbonyl, carboxylic and guaiacyl groups over sulfided $CoMo/\gamma - Al_2O_3$ and $NiMo/\gamma - Al_2O_3$ catalysts. 1. Catalytic reaction schemes. *Applied catalysis A* 109: 77-96.

[22] Furimsky. E. (1983). Chemistry of catalytic hydrodeoxygenation. *Catalysis Reviews* 25 (3) 421-458.

[23] Mortensen et al. (2011). A review of catalytic upgrading of bio-oil to engine fuels. *Applied catalysis A: General* 407: 1-19.

[24] alsglobal.se, (2016). *Analystekniker* [online] Available at: `https://www.alsglobal.se/als-scandinavia/analystekniker` [Accessed January-17]

[25] airproducts.com, (2017). *Analytical laboratories applications* [online] Available at: `http://www.airproducts.com/industries/Analytical-Laboratories/analytical-lab-applications/product-list/gas-chromatography-gc-analytical-laboratories.aspx?itemId=E04BB35D53DE44E8B751BA27B577AC43` [Accessed January-17]

[26] airproducts.com, (2017). *Analytical laboratories applications* [online] Available at: `http://www.airproducts.com/industries/Analytical-Laboratories/analytical-lab-applications/product-list/gc-with-flame-ionization-detector-gc-fid-analytical-laboratories.aspx?itemId=D6D6641C668A47139A6F1960D9441B93` [Accessed January-17]

[27] hiq.linde-gas.com, (2017). *thermal conductivity detector (TCD)* [online] Available at: `http://hiq.linde-gas.com/en/analytical_methods/gas_chromatography/thermal_conductivity_detector.html` [Accessed January-17]

[28] airproducts.com, (2017). *Analytical laboratories applications* [online] Available at: `https://www.airproducts.com/industries/Analytical-Laboratories/analytical-lab-applications/product-list/gc-with-thermal-conductivity-detector-gc-tcd-analytical-laboratories.aspx?itemId=651A80DACEBF49F4993E7C447B42808E` [Accessed January-17]

[29] thermofisher.com, (2016). *Overview of mass spectrometry for protein analysis* [online] Available at: https://www.thermofisher.com/se/en/home/life-science/protein-biology/protein-biology-learning-center/protein-biology-resource-library/pierce-protein-methods/overview-mass-spectrometry.html.html [Accessed January-17]

[30] livescience.com, (2016). *States of matter: Plasma* [online] Available at: http://www.livescience.com/54652-plasma.html [Accessed january-17]

[31] Micromeritics.com. *Gas adsorption theory.* Available at: http://www.micromeritics.com/Repository/Files/Gas_Adsorption_Theory_poster.pdf [Accessed january-17]

[32] parrinst.com. *Gaskets and seals.* Available at: http://www.parrinst.com/products/stirred-reactors/options-accessories/gaskets-and-seals/ [Accessed january-31]

[33] wermac.org. *Introduction to valves - rupture disc.* Available at: http://www.wermac.org/valves/valves_rupture_disk.html [Accessed january-31]

A

Appendix

The appendix starts with a flow sheet of the system designed in HYSYS and a visual presentation of the freeze drying process of the catalyst. Thereafter the GC analysis results are presented with the FID and TCD for each experiment. The number of experiment labeled inside the figures is wrong. The simulated concentration profiles for the gas phase in Matlab are presented last.

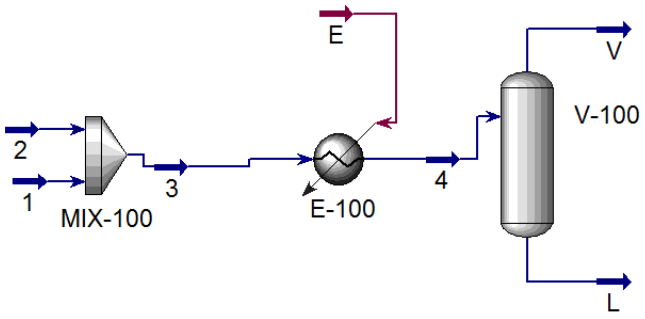

Figure A.1: Flow sheet of system used for calculating solubility of H_2 in n-Dodecane

Figure A.2: visual presentation of the freeze drying step of the catalyst

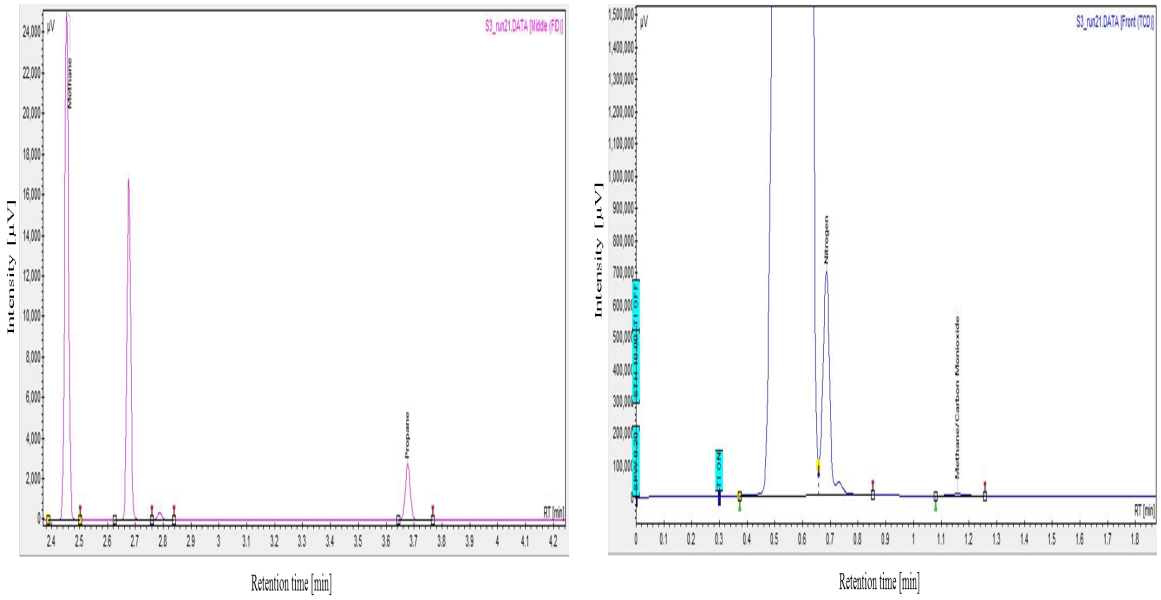

Figure A.3: GC results for experiment 2 with T at 320°C. FID (left), TCD (right)

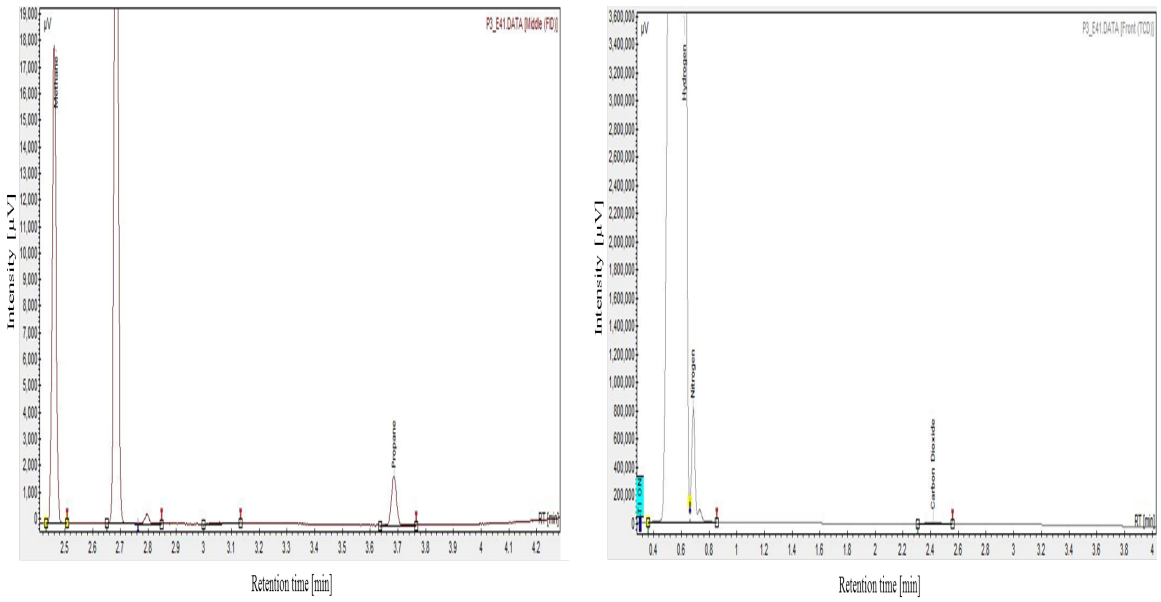

Figure A.4: GC results for experiment 3 with P at 40 bar. FID (left), TCD (right)

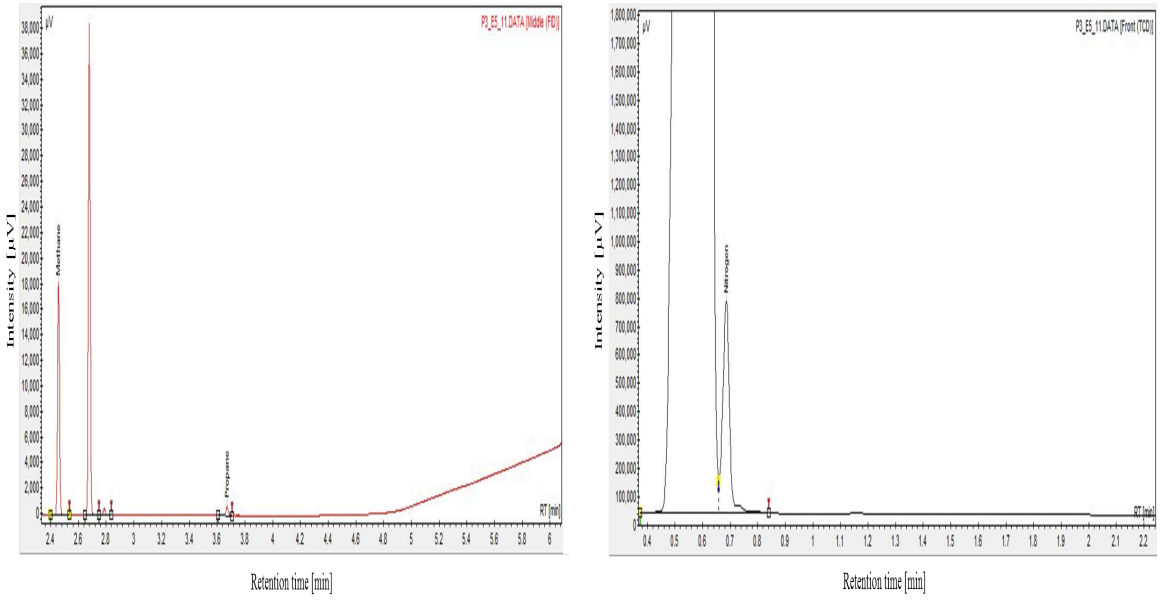

Figure A.5: GC results for experiment 4 with 2wt.% conc. of S.A. FID (left), TCD (right)

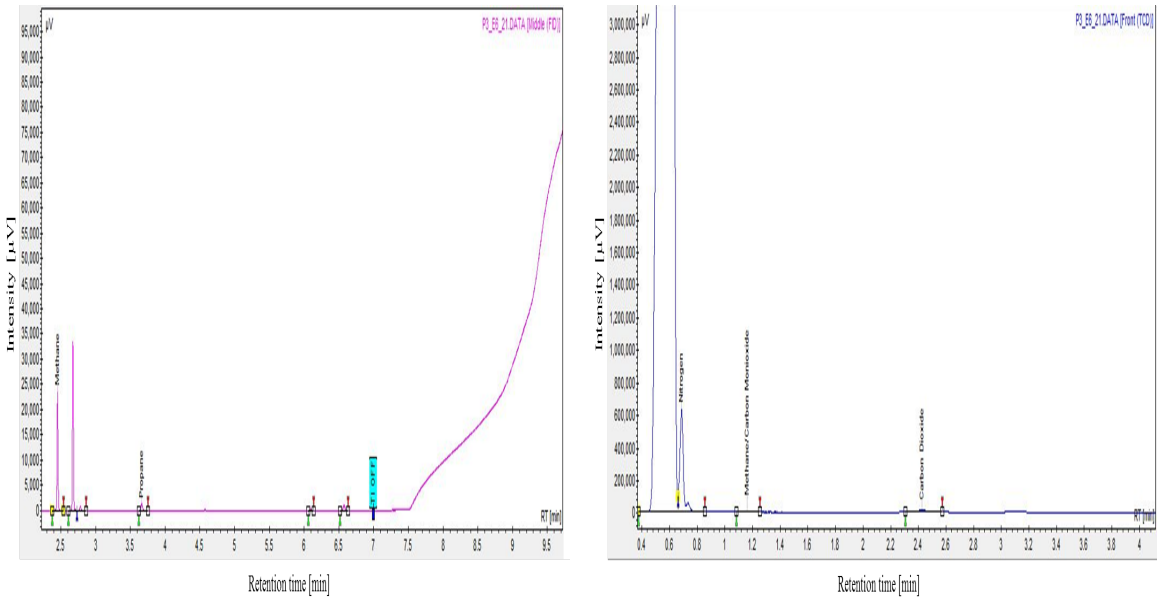

Figure A.6: GC results for experiment 5 with P at 60 bar. FID (left), TCD (right)

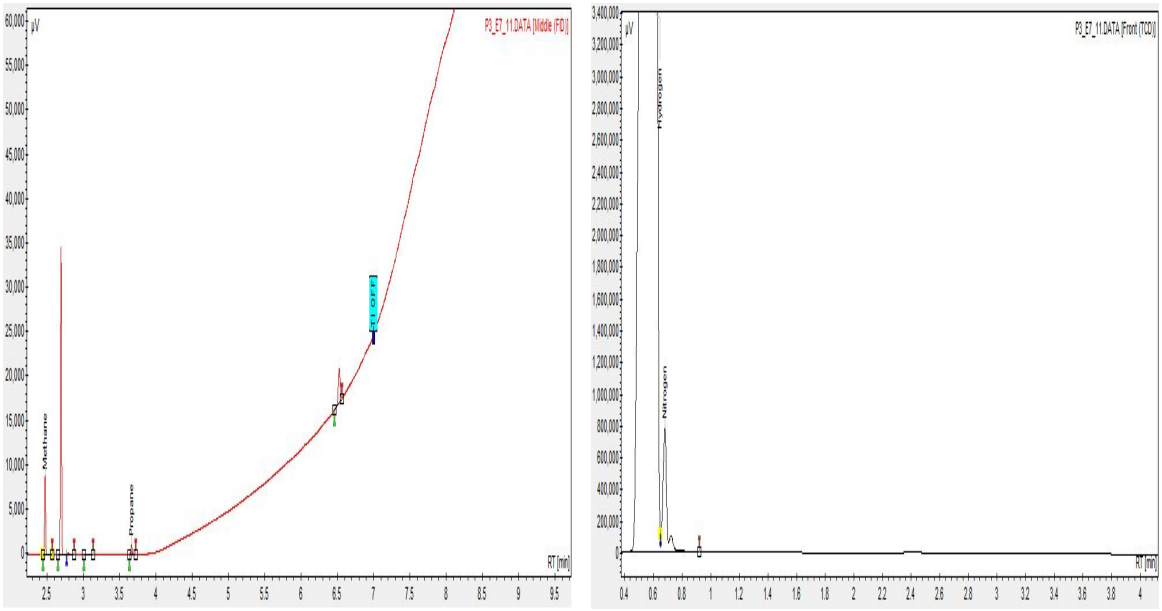

Figure A.7: GC results for experiment 6 with T at 280°C. FID (left), TCD (right)

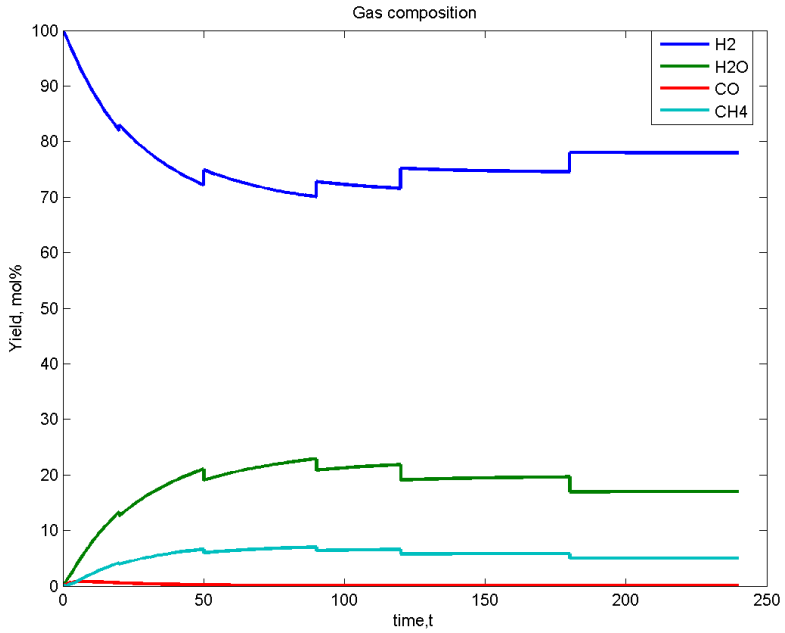

Figure A.8: shows the simulated gas concentration profiles at T:320°C, P:50 bar, C:5 wt.%

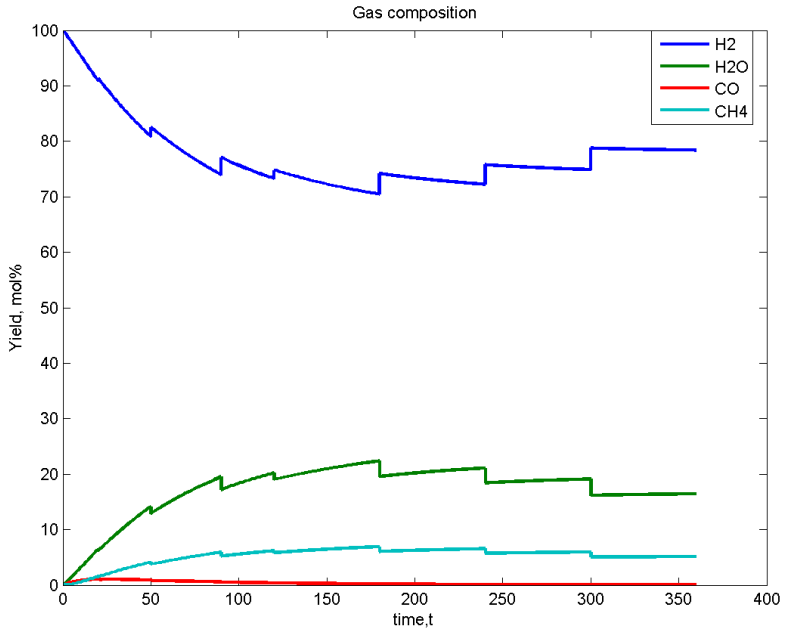

Figure A.9: shows the simulated gas concentration profiles at T:300°C, P:40 bar, C:5 wt.%

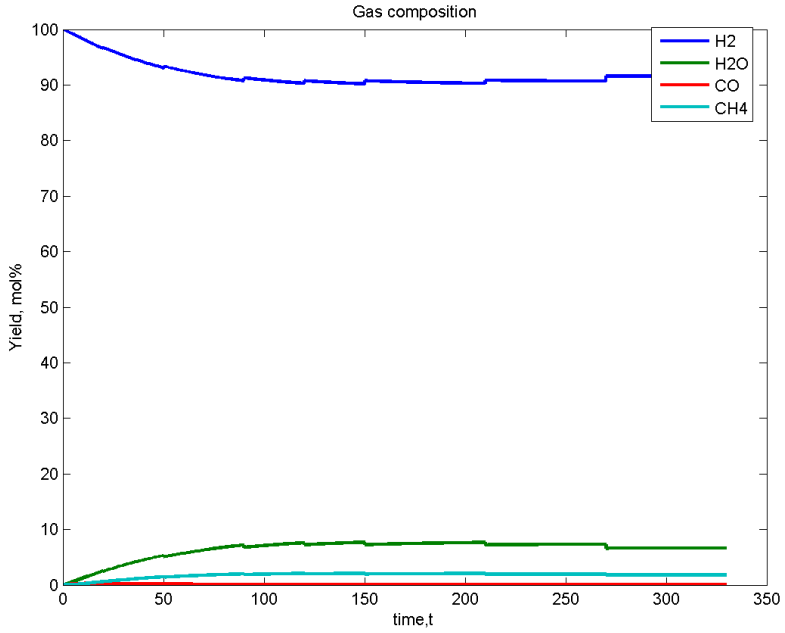

Figure A.10: shows the simulated gas concentration profiles at T:300°C, P:50 bar, C:2 wt.%

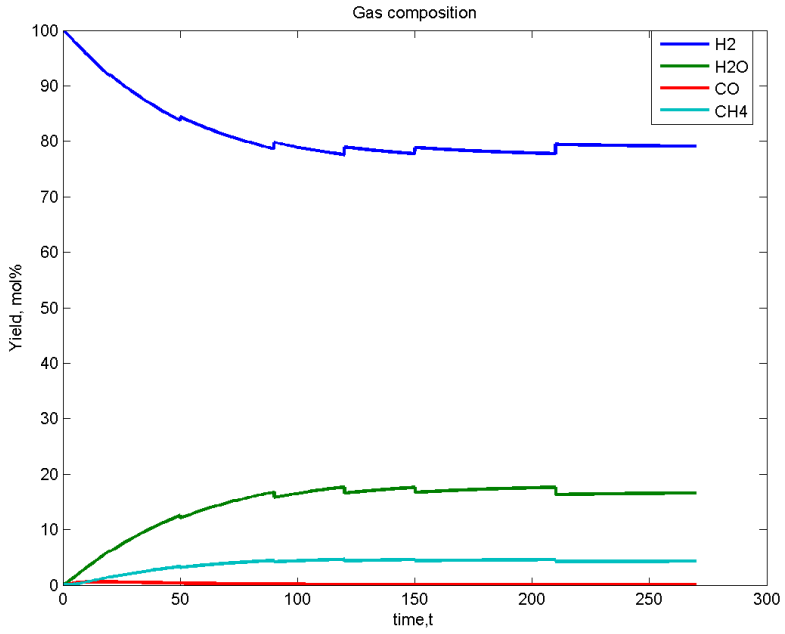

Figure A.11: shows the simulated gas concentration profiles at T:300°C, P:60 bar, C:5 wt.%

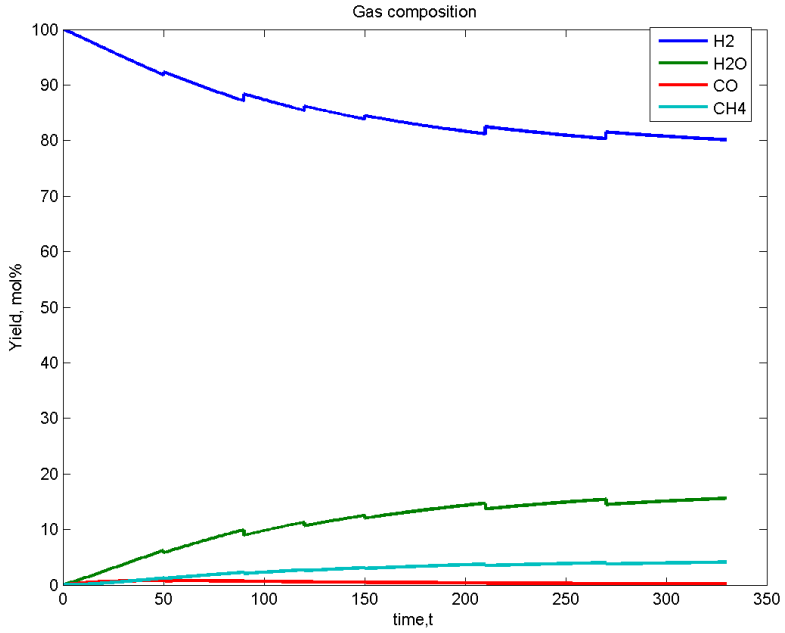

Figure A.12: shows the simulated gas concentration profiles at T:280°C, P:50 bar, C:5 wt.%